(This is a sample cover image for this issue. The actual cover is not yet available at this time.)

Journal of South American Earth Sciences 34 (2012) 10–25

Contents lists available at SciVerse ScienceDirect

Journal of South American Earth Sciences

journal homepage: www.elsevier.com/locate/jsames

Age and magmatic evolution of the Famatinian granitic rocks of Sierra de Ancasti, Sierras Pampeanas, NW Argentina

Juan A. Dahlquist [a,b,*], Carlos W. Rapela [c], Robert J. Pankhurst [d], C. Mark Fanning [e], Jeffrey D. Vervoort [f], Garret Hart [f], Edgardo G. Baldo [a], Juan A. Murra [a], Pablo H. Alasino [b,g], Fernando Colombo [a,b]

[a] CICTERRA-CONICET-UNC, Av. Vélez Sarsfield 1611, Pab. Geol., X5016CGA Córdoba, Argentina
[b] INGeReN-CENIIT-UNLaR. Av. Gob. Vernet y Apostol Felipe. 5300, La Rioja, Argentina
[c] CIG-CONICET-UNLP, Calle 1 N° 644, 1900 La Plata, Argentina
[d] British Geological Survey, Keyworth, Nottingham NG12 5GG, United Kingdom
[e] Research School of Earth Sciences, The Australian National University, Canberra, Australia
[f] School of Earth and Environmental Sciences, Washington State University, PO Box 642812, Pullman, WA 99164-2812, USA
[g] CRILAR-CONICET, Anillaco Entre Ríos y Mendoza, 5301, Anillaco, La Rioja, Argentina

ARTICLE INFO

Article history:
Received 23 February 2011
Accepted 23 July 2011

Keywords:
U–Pb SHRIMP and LA-ICP-MS ages
I-type granite
Fractional crystallization

ABSTRACT

The granitic rocks of the Sierra de Ancasti represent one of the easternmost outcrops of the Famatinian arc of the Sierras Pampeanas. We report here new U–Pb SHRIMP and LA-ICP-MS Ordovician ages and a petrological and geochemical study of the Las Cañadas I-type granitic complex in the central sector of Sierra de Ancasti. Numerical modelling indicates that calc-alkaline and metaluminous monzogranites (SiO_2 = 69.8–73.0 wt.%) were produced by fractional crystallization of plagioclase-rich tonalite (~60% plagioclase and SiO_2 = 60.9–62.5 wt.%) from an inferred parental magma of granodioritic composition (SiO_2 = 67.4 wt.%). Sm–Nd isotopic data on the dated rocks indicate a dominant continental crustal input, as reported for other Ordovician granitic rocks (Famatinian magmatism) farther west in the Sierras Pampeanas. Combined ages and isotopic data are consistent with previous studies indicating that Famatinian magmatism was short-lived (~20 Ma) and lacked a significant asthenospheric contribution. The occurrence of inherited zircon and the petrological and geochemical data from the Las Cañadas complex indicate that the parental magma was derived from mixed igneous and sedimentary material in the source or by partial melting of igneous rocks of different ages. Systematic dating of inherited zircon cores is required to clarify this issue. Zircon saturation geothermometry combined with geochemical data indicates that the onset of zircon crystallization, together with variable amounts of other minerals such as plagioclase, quartz, biotite, oxides and apatite, occurred when the parental magma reached 67 wt.% SiO_2 with ~440 ppm of Zr at ~878 °C.

1. Introduction

The Sierras Pampeanas of NW Argentina are a series of mountainous ranges, comprising crystalline basement intruded by diverse Palaeozoic igneous rocks and elevated during Miocene-to-recent compressional (Andean) tectonics (e.g. Jordan and Almendinger, 1986) (Fig. 1). The igneous rocks were generated in four main magmatic events: (a) Pampean (latest Neoproterozoic–mid Cambrian; Rapela et al., 1998, 2007), (b) Famatinian (early–mid Ordovician; Aceñolaza et al., 1996; Pankhurst et al., 1998, 2000; Miller and Söllner, 2005; Büttner et al., 2005; Dahlquist and Galindo, 2004; Dahlquist et al., 2008), (c) Achalian (mid-late Devonian; Dorais et al., 1997; Sims et al., 1998; Stuart-Smith et al., 1999; Siegesmund et al., 2004; Rapela et al., 2008), and (d) Early Carboniferous (Grosse et al., 2009; Dahlquist et al., 2010). Despite this extensive literature, there are still regions where the petrogenesis of Ordovician granitic rocks has not been unequivocally defined; this is the case of the granitic rocks of the Sierra de Ancasti.

In this paper, we report the first U–Pb SHRIMP and LA-ICP-MS ages on zircon, and assess petrography, mineral chemistry, bulk major and trace element compositions, and Sm–Nd isotopic data for the metaluminous granitic rocks of the *Las Cañadas granitic complex*. In order to define the main differentiation process during crystallization of the complex, we provide numerical models using major and trace element compositional data. We also evaluate the temperature of crystallization of the metaluminous rocks (using zircon saturation thermometry, T_{Zr}), together with the compositional evolution of the magma.

* Corresponding author. CICTERRA-CONICET-UNC, Av. Vélez Sarsfield 1611, Pab. Geol., X5016CGA Córdoba, Argentina. Tel.: +54 351 434 4980; fax: +54 351 433 3199.
E-mail address: jdahlquist@efn.uncor.edu (J.A. Dahlquist).

0895-9811/$ – see front matter © 2011 Elsevier Ltd. All rights reserved.
doi:10.1016/j.jsames.2011.07.006

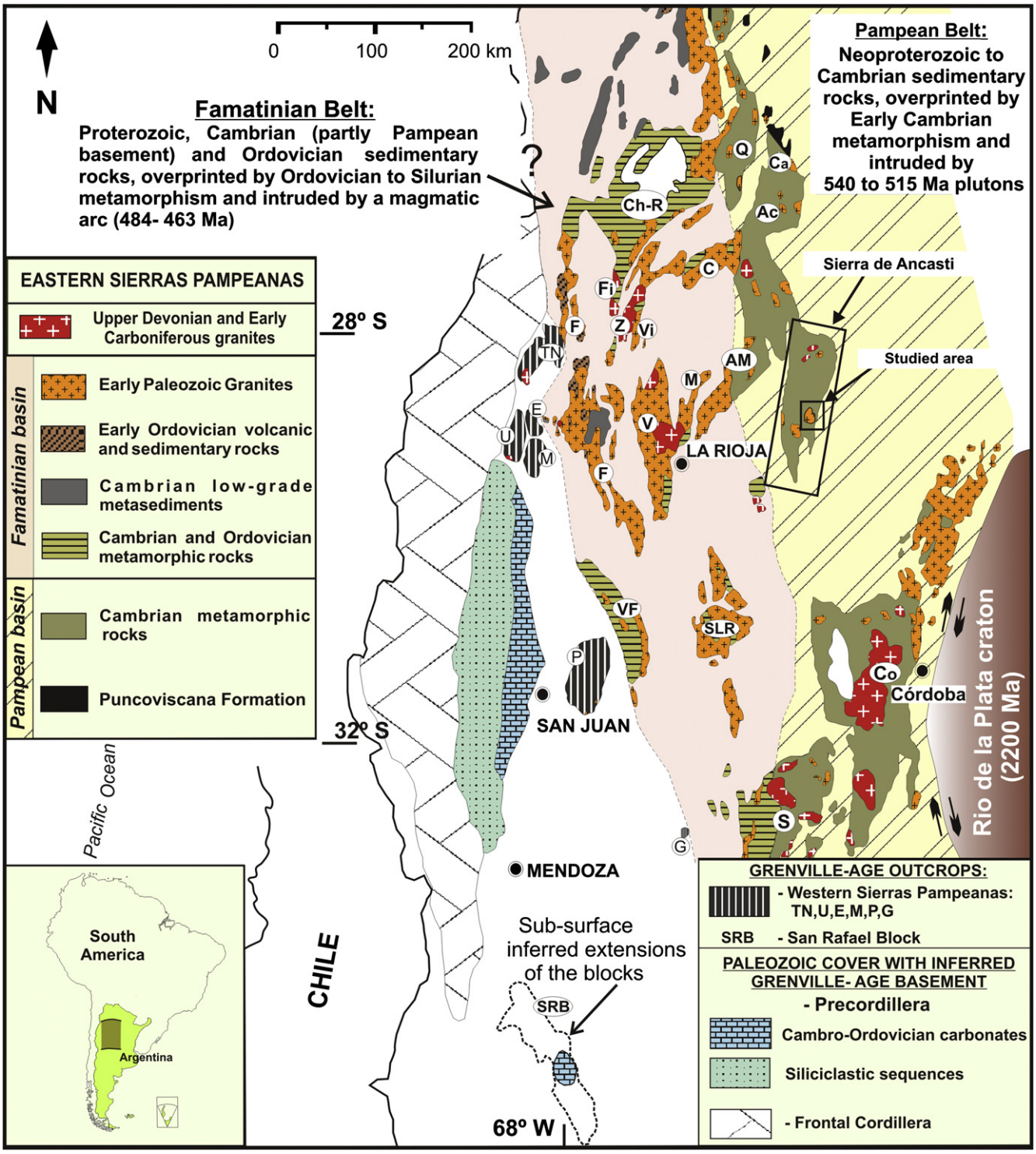

Fig. 1. Location of Sierra de Ancasti in the regional framework of the Sierras Pampeanas, NW Argentina (after Rapela et al., 2010). The rectangle shows the studied area. Main mountain ranges are: (Q) Quilmes, (Ch-R) Chango Real, (Ca) Calchaquíes, (Ac) Aconquija, (C) Capillitas, (Fi) Fiambalá, (Z) Zapata, (Vi) Vinquis, (A) Ancasti, (V) Velasco, (M) Mazán, (F) Famatina, (TN) Toro Negro, (U) Umango, (M) Maz, (E) Espinal, (P) Pie de Palo, (VF) Valle Fértil, (SLR) Southern La Rioja (including Los Llanos, Chepes and Ulapes), (Co) Córdoba, (S) San Luis, (G) Gigantes, (SRB) San Rafael Block. The limits of the Río de la Plata craton towards the Sierras de Córdoba is inferred from geophysical studies and boreholes drilled for oil exploration (Rapela et al. 2007).

2. Geological setting

The dominant granitic composition in the Sierra de Ancasti is calc-alkaline and metaluminous (Fig. 2). These granitic rocks were emplaced in a metamorphic basement composed of low- to high-grade schist and gneiss (Reissinger, 1983; Rapela et al., 2005). As established by the data presented here, the metaluminous granitoids of the Sierra de Ancasti were emplaced during the early part of the Ordovician Period (see Section 8) as part of the Famatinian magmatic arc along the proto-Andean margin of Gondwana.

The Famatinian arc was developed on continental crust as argued by Pankhurst et al. (1998) and Dahlquist and Galindo (2004)

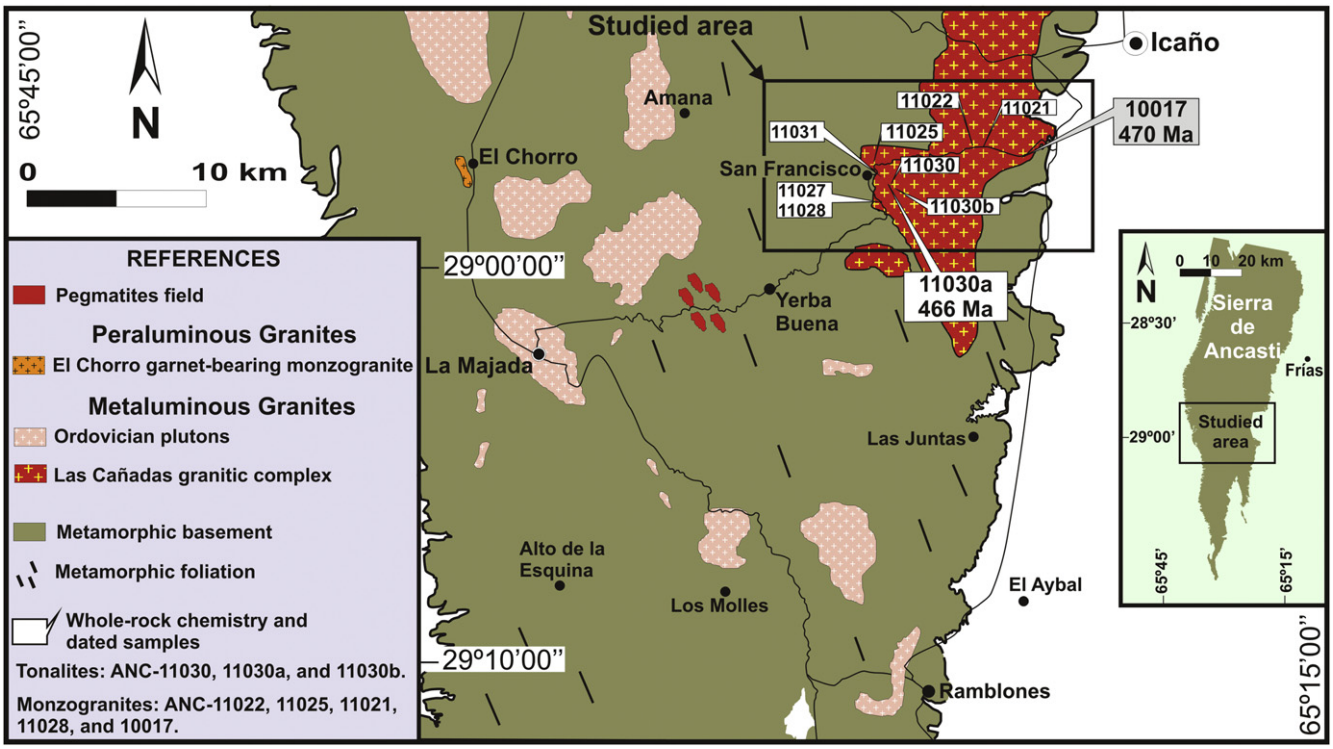

Fig. 2. Simplified geological map of the central sector of the Sierra de Ancasti. Samples included in Tables 1, 2 and 4 are shown in the geological map. ANC-10017 (monzogranite) and ANC-11030a (tonalite) are granitic rock with U–Pb SHRIMP and LA-ICP-MS ages determined in this work, respectively.

and accepted widely (e.g., Miller and Söllner, 2005). In the Famatinian magmatic belt of the Sierras Pampeanas, Pankhurst et al. (2000) identified three distinct granite types (Fig. 1): dominant I-type, small-scale S-type, and tonalite–trondhjemite–granodiorite (TTG, confined to the Sierras de Córdoba, Fig. 1). These three granite types can be distinguished petrologically, geochemically and spatially, although all were essentially contemporaneous within the 484–463 Ma interval (see also Dahlquist et al., 2008). Detailed petrological and geochemical studies of these rocks are given by Aceñolaza et al. (1996), Saavedra et al. (1998), Pankhurst et al. (1998, 2000), Dahlquist and Galindo (2004), Miller and Söllner (2005), Dahlquist (2002), Dahlquist et al. (2005, 2007, 2008).

The widespread Famatinian magmatism yielded extensive I-type intrusions (mostly tonalite, granodiorite and minor monzogranite and gabbro) with $\varepsilon Nd_t = -3$ to -6 (data from Pankhurst et al., 1998, 2000; Dahlquist and Galindo, 2004; Dahlquist et al., 2008). Some gabbros in the Sierra de Valle Fértil reached a more radiogenic value of $\varepsilon Nd_t = -2.4$, and subordinate isolated Ordovician plutons of Na-rich granite located in the Pampean belt foreland (TTG suites) have $\varepsilon Nd_t = +1.6$ to -0.2. Most of the granitic rocks have T_{DM} model ages between 1.7 and 1.5 Ga and Nd isotopic signatures suggesting derivation from a composite Palaeo–Mesoproterozoic lithospheric section that included lower and upper crust sources as well as the sub-lithospheric mantle (Rapela et al., 2008; Dahlquist et al., 2008 and references therein). Thus, with the exception of the minor TTG suites, the Famatinian magmatic arc reworked old lithospheric sources, with very little addition of juvenile material.

Dahlquist et al. (2008) concluded that: (i) the Famatinian magmatism was brief (~484–~463 Ma), in remarkable contrast to the long-lived Mesozoic–Cenozoic cordilleran magmatism of the Andes; and (ii) the Early to mid Ordovician development of ensialic marine basins was synchronous with the emplacement of conspicuous lithosphere-derived magmatism in the central region of the Famatinian orogenic belt, which strongly contrasts with the Andean-type model for the production of magmas (Dahlquist and Galindo, 2004). During the Mid Ordovician the magmatism was completely extinguished and the sedimentary basins closed in the early Late Ordovician. A previous Rb–Sr age of 435 Ma reported for Sierra de Ancasti granites by Knüver (1983) is significantly younger (Silurian) but our work here confirms that the Las Cañadas granitic complex is indeed of typical Famatinian age (Ordovician).

3. Background geology of Sierra de Ancasti

The Sierra de Ancasti occurs in the eastern sector of the Famatinian orogenic belt (Fig. 1), in southeastern Catamarca province, and it is formed by three distinctive metamorphic domains. The *eastern flank* is composed of paragneiss and migmatites (the Jumeal member of the Sierra Brava complex, Aceñolaza and Toselli, 1977) as well as marbles, schists and amphibolites (the La Calera member). The *central sector* is mostly formed by banded schists of the Ancasti Formation (Aceñolaza and Toselli, 1977; Willner, 1983a). These rocks define a homoclinal folded sequence 10–11 km thick, with a regional foliation that strikes NNW–SSE and dips 50–70°E. The schists record a low-pressure M-1 metamorphism (Ms + Bt + And + Crd, mineral abbreviations from Kretz, 1983) that was overprinted by a syn-deformational M-2 event of medium grade (Willner, 1983b). The M-1 metamorphism is assigned to the Pampean orogen through a Rb–Sr mineral isochron of 524 ± 28 Ma (Knüver, 1983). Calc-silicate layers of Qtz + Cal + Pl + Ep + Grt + Bt + Hbl are interleaved in the schists. In the *western flank* of the sierra, metasediments of the Ancasti Formation prograde to gneisses and migmatites with Crd + Bt + Sil + Kfs ± Grt and are called the El Portezuelo Formation (Willner, 1983a).

Granitic rocks of Ordovician age and a pegmatite complex with tourmaline and beryl are emplaced in the Sierra Brava complex and the Ancasti Formation. Reissinger (1983) has reported petrographic, geochemical, geochronological and isotopic data for the granitic

Table 1a
Representative composition of plagioclase in the biotite-bearing tonalite of the Las Cañadas granitic complex from electron microprobe (JEOL JXA 8500F *Hyperprobe*).

Sample	ANC-11030				
Analysis number	209	210	213	225	Average[a]
wt.%					
SiO_2	56.46	55.97	55.68	55.43	55.89
Al_2O_3	27.19	27.75	27.91	27.61	27.62
CaO	9.04	9.42	9.73	9.23	9.36
Na_2O	7.08	6.68	6.72	6.73	6.8
K_2O	0.1	0.11	0.12	0.13	0.12
Total	99.87	99.93	100.16	99.13	99.79
Ab	58.3	55.9	55.2	56.5	56.4
An	41.1	43.5	44.2	42.8	42.9
Or	0.5	0.6	0.7	0.7	0.7

Abbreviations: Ab = Albite, An = Anortite, Or = Orthoclase.
[a] Plagioclase composition used in the fractional crystallization model using major oxides (Table 6).

Table 1b
Representative composition of biotite in the biotite-bearing tonalite of the Las Cañadas granitic complex from electron microprobe (JEOL JXA 8500F *Hyperprobe*).

Samples	ANC-11030				
Analysis number	214	215	220	223	Average[a]
wt.%					
SiO_2	34.46	34.73	34.75	34.37	34.58
TiO_2	2.60	2.58	2.82	2.79	2.70
Al_2O_3	16.69	16.59	16.5	16.54	16.58
FeO	20.36	20.33	20.77	19.7	20.29
MnO	0.4	0.38	0.46	0.4	0.41
MgO	9.49	9.29	9.35	9.97	9.52
CaO	0.05	0.05	0.04	0.02	0.04
Na_2O	0.13	0.38	0.07	0.09	0.17
K_2O	9.58	9.64	9.81	9.87	9.73
F	0.14	bdl	bdl	bdl	bdl
Total	93.90	93.97	94.57	93.75	94.05
F=O	0.06	0.00	0.00	0.00	0.00
CTotal	93.84	93.97	94.57	93.75	94.03
Structural formulae calculated on basis 22 O					
Al^{IV}	*2.59*	*2.56*	*2.58*	*2.61*	*2.59*
$Fe^{2+}/(Fe^{2+}+Mg)$	*0.55*	*0.55*	*0.55*	*0.53*	*0.55*

Total iron expressed as FeO.
CTotal = Calculated Total.
bdl = below detection limit.
[a] Biotite composition used in the fractional crystallization model using major oxides (Table 6).

rocks of the Sierra de Ancasti. Based on the presence of normative corundum and following the White and Chappell (1977) nomenclature, Reissinger (1983) suggested derivation by partial melting of metasediments or I-type magmas with large-scale assimilation of metamorphic rocks leading to the enrichment of Al. In the central area of the Sierra de Ancasti, where the Las Cañadas and La Majada granitic complexes crop out (Fig. 2), Reissinger (1983) observed the association of quartz-rich diorite, granodiorite with amphibole and biotite, and two-mica granite, which he considered to be genetically related, although he did not propose a specific genetic model. Cisterna (2003) studied the La Majada granitic complex (Fig. 2), indicating the association of gabbro and diorite, tonalite, granodiorite, and monzogranite (with muscovite after biotite).

4. Analytical methods

Numerous samples were collected from the Las Cañadas granitic complex, of which 30 were selected for petrographic investigations. Based on these results and our previous investigations (including large field observations and petrographic studies), we chose 8 representative samples from an E–W cross-section across the entire granitic complex for geochemical, chemical mineral, isotope, and geochronological analysis. Whole-rock major and trace element compositions were determined by ICP-OES and ICP-MS (following the 4-Lithoresearch procedure), at Activation Laboratories, Ontario, Canada (ACTLABS). Following lithium metaborate/tetraborate fusion samples are dissolved in a weak nitric acid solution. Major elements, Be, Sc, V, Sr, Ba, and Zr are determined by Inductively Couple Plasma – Optical Emission Spectroscopy (ICP–OES). All other trace elements are determined by Inductively Coupled Plasma – Mass Spectrometry (ICP–MS).

Mineral chemistry was determined on representative rock samples using two electron microprobes. A JEOL JXA 8500F *Hyperprobe* equipped with 5 tuneable wavelength dispersive spectrometers at the School of Earth and Environmental Sciences (SEES), Washington State University (WSU) (Pullman, USA). The beam current was 15 kV, probe current of 20 nA, and the beam diameter was 5 μm. Absolute abundance for each element was determined by comparison with standards (Jarosewich et al., 1980; McGuire et al., 1992). A JEOL JXA-8900-M *Superprobe* equipped with five crystal spectrometers at the Luis Brú Electron Microscopy Center, Complutense University, Madrid, Spain. Operating conditions were: acceleration voltage of 15 kV, probe current of 20 nA, with a beam diameter between 1 and 2 μm. An on-line ZAF program or Phi–Rho–Z algorithm (Armstrong, 1988) was used with the JEOL JXA 8500F *Hyperprobe* and an on-line ZAF program was used with the JEOL JXA-8900-M *Superprobe*. The data obtained from each electron microprobe are indicated in the Tables containing mineral chemical data.

Sm–Nd determinations of the two representative dated granitic units samples were carried out at the SEES, WSU. For Nd whole-rock isotopic analyses, ~0.25 g aliquots of whole-rock powders were dissolved at high pressure in sealed, steel-jacketed teflon bombs with a 10:1 mixture of concentrated HF and HNO_3 acids at 150 °C for 5–7 days. After conversion from fluorides to chlorides, samples were spiked with mixed ^{149}Sm–^{150}Nd tracers. LREEs were initially separated on cation exchange columns using AG 50W-X8 (200–400 mesh) resins. Nd and Sm were separated from the LREE aliquot on columns with HDEHP-coated teflon powder and HCl (Vervoort and Blichert-Toft, 1999).

All analyses were conducted on a Thermo-Finnigan Neptune MC-ICP-MS at the SEES, WSU. Nd analyses were corrected for mass

Table 1c
Representative composition of Fe-oxides and apatite in the biotite-bearing tonalite of the Las Cañadas granitic complex from electron microprobe (JEOL JXA 8500F *Hyperprobe*).

Sample	ANC-11030						
	Magnetite			Ilmenite		Apatite	
Analysis number	221	222[a]	86	216[a]	217	224	495[a]
wt.%							
SiO_2	0.32	0.24	0.21	0.86	0.20	0.66	0.57
TiO_2	bdl	0.01	0.00	47.70	46.44	0.00	0.08
Al_2O_3	0.10	0.05	0.14	0.27	0.00	0.16	0.11
Fe_2O_3	98.98	98.53	99.80	42.86	45.83	0.39	0.33
MnO	0.08	0.10	0.04	0.03	0.05	0.12	0.09
MgO	0.06	0.04	0.02	5.86	5.58	0.13	0.08
CaO	0.01	0.01	0.02	0.58	0.02	54.22	55.17
P_2O_5						41.08	40.96
F						5.12	4.65
Total	99.52	98.91	100.24	98.15	98.12	101.88	102.04
F=O						2.16	1.96
CTotal	99.52	98.91	100.24	98.15	98.12	99.72	100.08

Total iron as Fe_2O_3.
bdl = below detection limit.
[a] Magnetite and ilmenite compositions used in the fractional crystallization model using major oxides (Table 6).

Table 1d
Representative composition of plagioclase and alkali feldspar in monzogranite of the Las Cañadas granitic complex from electron microprobe (JEOL JXA-8900-M *Superprobe*).

Sample	ANC-11022			
Mineral	Plagioclase			Alkali feldspar
Analysis number	18	19	20	16
wt.%				
SiO_2	60.10	61.15	60.44	63.86
Al_2O_3	24.77	24.18	24.82	18.52
CaO	6.27	5.96	6.67	0.06
Na_2O	7.98	8.13	7.78	0.54
K_2O	0.08	0.08	0.07	16.34
Total	99.19	99.50	99.77	99.32
Ab	*69.4*	*70.9*	*67.6*	*4.8*
An	*30.1*	*28.7*	*32.0*	*0.3*
Or	*0.5*	*0.5*	*0.4*	*94.9*

fractionation using $^{146}Nd/^{144}Nd = 0.7219$ and normalized using Ames and La Jolla Nd standards. Sm analyses were corrected for fractionation using $^{147}Sm/^{152}Sm = 0.56081$. All mass fractionation corrections were performed using the exponential law.

The uncertainties on Nd isotopic measurements reflect in-run error only and are presented as two standard errors are reported by Bouvier et al. (2008, Tables 2 and 3). The full uncertainties are better assessed from the reproducibility of the standards. Average reproducibility (2 standard deviations) of $^{143}Nd/^{144}Nd$ on Ames standard during the period of analysis was ±0.000020.

U–Pb SHRIMP and LA-ICP-MS ages of two representative granitic facies (Fig. 2 and Table 2) were obtained from: (i) ANC-10017 a typical monzogranite and (ii) ANC-11030a a biotite-bearing tonalite, both granitic facies included in the Las Cañadas granitic complex (see Section 5.2.1.). Separated zircons from ANC-10017 were analysed for U–Pb isotopic composition using SHRIMP II at the Australian National University, Canberra, following methods given in Williams (1998), and references therein. LA-ICP-MS analysis of separated zircons from ANC-11030a and ANC-11022 was carried out at the School Earth and Environmental Sciences Washington State University (Pullman, USA), using a New Wave Nd:YAG UV 213 nm laser coupled to a Thermo–Finnigan Element 2 single collector, double-focussing, magnetic sector ICP-MS. Operating procedures and parameters are discussed in greater depth by Gaschnig et al. (2010). Fractionation in the plasma was corrected by normalizing U/Pb and Pb/Pb ratios of the unknowns to the zircon standards (Chang et al., 2006). For this study we used two zircon standards: Peixe, with an age of 564 Ma (Dickinson and Gehrels, 2003), and FC-1, with an age of 1099 Ma (Paces and Miller, 1993).

Table 1e
Representative composition of biotite in monzogranite of the Las Cañadas granitic complex from electron microprobe (JEOL JXA-8900-M *Superprobe*).

Sample	ANC-11022		
Mineral	Biotite		
Analysis number	14	26	25
wt.%			
SiO_2	35.12	35.74	35.58
TiO_2	3.46	3.31	3.05
Al_2O_3	16.45	16.82	16.46
FeO	21.10	21.40	19.20
MnO	0.37	0.49	0.44
MgO	8.84	8.37	9.13
CaO	0.07	bdl	0.04
Na_2O	0.04	0.05	0.03
K_2O	9.80	9.96	9.83
Total	95.27	96.13	93.79
Structural formulae calculated on basis 22 O			
Al^{IV}	*2.56*	*2.52*	*2.46*
$Fe^{2+}/(Fe^{2+} + Mg)$	*0.57*	*0.59*	*0.54*

Total iron expressed as FeO. F is below the detection limit ranging from 436 to 659 ppm.

Table 1f
Representative composition of magmatic muscovite in the El Chorro garnet-bearing monzogranite from electron microprobe (JEOL JXA 8500F *Hyperprobe*) and secondary muscovite in the monzogranite of the Cañadas granitic complex.

Samples	ANC-11038	ANC-11022		
Analysis number	Average	21	22	24
wt.%				
SiO_2	44.49	46.56	45.96	45.47
TiO_2	0.56	0.94	2.05	0.55
Al_2O_3	35.27	30.22	28.70	29.71
FeO	2.04	4.48	5.11	5.27
MnO	0.02	bdl	bdl	bdl
MgO	0.62	1.48	1.50	1.53
CaO	0.02	0.08	0.03	0.01
Na_2O	0.59	0.19	0.13	0.23
K_2O	10.77	10.86	10.96	11.22
F	0.01	bdl	bdl	bdl
Total	94.38	94.85	94.42	93.98
F=O	0	–	–	–
CTotal	94.38	94.85	94.42	93.98
Structural formulae calculated on basis 22 O				
Al^{IV}	*1.97*	*1.64*	*1.66*	*1.68*
$Fe^{2+}/(Fe^{2+} + Mg)$	0.65	0.63	0.66	0.66

Total iron expressed as FeO.
CTotal = Calculated Total.
bdl = below detection limit.
ANC-11038: El Chorro garnet-bearing monzogranite; ANC-11022: Monzogranite of the Las Cañadas granitic complex.
Representative composition of magmatic muscovite in the El Chorro garnet-bearing monzogranite from Dahlquist et al. (2011).

5. Petrology, mineral and whole-rock chemistry

5.1. Field occurrence and mesoscopic description

The Las Cañadas granitic complex, the largest igneous body (4 × 11 km) in the Sierra de Ancasti (Figs. 1 and 2), is discordant to ~NE–SW structural trends (20°–30°) in the metamorphic rocks (gneiss and schist), of which it contains large xenoliths (Fig. 3a,b).

Based on field, petrographic and geochemical data, two main facies are recognised: (i) dominant monzogranite and (ii) subordinate tonalite forming small outcrops of metric size. The monzogranite contains scattered phenocrysts of alkali feldspar (5–2 mcm long) in an equigranular matrix formed by Pl + Qtz + Bt + Ms (secondary). The tonalite is equigranular and mesocratic with amphibole and biotite, or biotite as the only mafic mineral. Occasionally, probable metamict allanite and titanite were observed. The monzogranitic facies is found throughout the entire granitic complex, whereas the tonalite is mainly constrained to the central–western sector, where it interdigitates with the monzogranite, defining sills of variable thickness with sharp and lobate contacts (Fig. 3a), suggesting similar time of emplacement.

Only the monzogranite contains inclusions of metamorphic xenoliths, indicating possible incorporation of metamorphic fragments during its ascent through middle–upper crust. The strong angular form of the xenoliths (Fig. 3b) negates the possibility of significant magmatic assimilation.

5.2. Petrography and mineral chemistry

5.2.1. Las Cañadas granitic complex

5.2.1.1. Tonalite. These rocks have equigranular texture with grain size ranging from 2 to 5 mm. The magmatic assemblage of the tonalite includes two subfacies (modal proportions %): (i) Pl

Table 2
Major and trace element data for the metaluminous rocks of the Las Cañadas granitic complex.

[a]Rock type	Biotite tonalite			Monzogranite					Granodiorite
Samples	ANC-11.030	[b]ANC-11.030a	ANC-11.030b	ANC-11.028	ANC-11.025	[b]ANC-10017	ANC-11.021	ANC-11.022	[c]IPM
wt.%									
SiO_2	62.09	60.92	62.48	69.77	70.61	71.87	72.98	71.75	67.40
TiO_2	0.83	0.80	0.80	0.42	0.39	0.26	0.25	0.32	0.55
Al_2O_3	18.18	18.25	17.79	15.20	14.79	14.53	14.44	14.57	16.19
$Fe_2O_3^{total}$	5.96	5.51	5.61	3.33	3.27	2.15	2.23	2.81	4.23
MnO	0.12	0.13	0.10	0.06	0.06	0.05	0.05	0.06	0.09
MgO	1.55	1.42	1.49	1.01	0.92	0.62	0.53	0.77	1.12
CaO	5.09	4.86	5.17	2.47	2.21	1.79	1.36	1.96	3.37
Na_2O	4.07	3.95	3.78	3.81	3.29	3.72	3.54	3.34	3.67
K_2O	1.73	1.84	1.61	3.51	3.80	3.83	3.91	3.79	2.86
P_2O_5	0.29	0.26	0.27	0.23	0.26	0.15	0.17	0.25	0.27
LOI	0.53	0.70	0.67	0.46	0.64	0.64	0.80	0.56	0.55
Total	100.45	98.64	99.77	100.27	100.23	99.61	100.26	100.18	100.30
ppm									
Cs	15.7	21.3	11.3	8.2	6.8	11.0	36.7	19.0	18
Rb	67	78	66	162	153	199	246	199	140
Sr	411	405	404	141	128	86	73	105	243
Ba	270	282	257	403	440	218	210	314	294
La	20.8	21.8	18.8	41.6	41.7	23.9	27.1	35.7	29.0
Ce	40.6	44.7	39.2	87.8	88.0	53.0	58.8	74.7	59.4
Pr	4.92	5.71	5.20	10.1	9.99	6.09	6.60	8.50	6.89
Nd	20.7	20.8	19.8	38.4	37.6	22.4	24.9	31.9	26.9
Sm	4.65	4.50	4.49	7.57	7.39	4.89	5.30	6.33	5.57
Eu	2.30	2.05	1.78	1.26	1.30	0.80	0.86	1.08	1.63
Gd	4.73	4.37	4.13	6.25	5.94	4.20	4.50	5.16	4.97
Tb	0.75	0.67	0.61	0.95	0.85	0.65	0.72	0.75	0.75
Dy	4.40	3.97	3.43	4.98	4.29	3.64	3.92	3.72	4.03
Ho	0.91	0.82	0.68	0.90	0.75	0.67	0.72	0.63	0.76
Er	2.73	2.45	2.05	2.57	2.15	1.92	2.07	1.77	2.20
Tm	0.42	0.38	0.32	0.37	0.31	0.29	0.30	0.26	0.34
Yb	2.96	2.58	2.18	2.37	1.99	1.86	1.96	1.71	2.27
Lu	0.51	0.42	0.37	0.35	0.30	0.28	0.29	0.25	0.37
U	3.52	1.09	1.33	2.24	2.41	4.40	1.99	2.15	2.77
Th	5.85	5.18	5.04	20.4	19.8	16.5	14.5	16.8	11.9
Y	23.7	21.6	17.9	26.6	21.3	20.7	20.9	17.6	20.4
Nb	9.70	11.8	9.70	13.1	10.8	12.2	12.3	13.8	12.0
Zr	751	838	833	210	231	142	143	185	440
Hf	16.4	18.4	18.7	5.4	6.1	4.1	4.0	4.9	10.1
Ta	0.85	0.86	0.40	1.36	1.15	1.90	2.10	2.12	1.55
Ga	22	22	21	21	20	16	19	20	21
Ge	1.4	1.5	1.1	1.5	1.3	1.0	1.8	1.4	1.4
ASI	1.06	1.09	1.06	1.09	1.14	1.10	1.19	1.16	1.11
AI	0.47	0.45	0.45	0.66	0.64	0.71	0.70	0.66	0.56
M				1.45	1.38	1.37	1.26	1.34	1.49
T_{Zr}(°C)				809	824	781	790	807	878

Abbreviations: ASI: Aluminium Saturation Index; AI: Agpaitic Index.
$T_{Zr} = 12{,}900/[2.95 + 0.85M + \ln(496{,}000/Zr_{melt})]$, where $D^{Zr,zircon/melt} = (496{,}000/Zr_{melt})$, is the ratio of Zr concentrations (ppm) in zircon to that in the saturated melt; M is a compositional factor that accounts for dependence of zircon solubility on SiO_2 and peraluminosity of the melt [(Na + K+ 2· Ca)/Al · Si), all in cation fraction]. Geothermometer was calibrated for $M = 0.9$ to 1.7. Equation and Zr concentrations (ppm) in zircon (=496,000 ppm) from Miller et al. (2003). The T_{Zr} calculation was not made for the tonalites as these were assumed to be adcumulates.
[a] According to the Q-A-P diagram of de La Roche (1992).
[b] Dated rocks.
[c] The inferred parental magma is a 45:55 mixture of a biotite-bearing tonalite (ANC-11030) and a monzogranite (ANC-11022), respectively.

(61.2) + Qtz (21.2) + Bt (14.2) and (ii) Pl (47.1) + Qtz (35.5) + Bt (10.2) + Hbl (3.0) with Zrn + Ap + oxides (Mag + Ilm, 1.13) and Zrn + Ap + $Ep_{primary}$ + Ttn + Mag ± Aln as accessory minerals, respectively. Our attention was focused in the biotite-bearing tonalites, which proved significant to understanding the differentiation process presented in Sections 6 and 9.

Plagioclase occurs as tabular and euhedral to subhedral crystals of rather constant size, with patchy or concentric zoning and polysynthetic twinning (Fig. 4a). Their compositions range from $Ab_{58.3}$ $An_{41.1}$ $Or_{0.5}$ to $Ab_{57.5}$ $An_{42.2}$ $Or_{0.3}$ (andesine, Table 1a). The abundance of plagioclase is remarkably high (~60%), demonstrating major plagioclase crystallization in this facies (Fig. 4a). Quartz forms anhedral crystals with undulose extinction and is homogeneously distributed.

Biotite (Table 1b) occurs as euhedral to subhedral tabular crystals with light to dark brown pleochroism. The biotites of the tonalite have moderate $Fe^{2+}/(Fe^{2+} + Mg)$ ratios (0.53–0.55) with measured siderophyllite–eastonite contents (2.56–2.61) (Table 1b). Zircon, fluor–apatite, oxide (magnetite and ilmenite, Table 1c) and occasionally scarce epidote are accessory minerals. Zircon occurs as scarce inclusions in biotite (small and medium crystals size ranging from 30 μm to 140 μm); systematic analysis using the electron microprobe indicates that this is the only radioactive mineral and monazite was not detected.

5.2.1.2. Monzogranite. The monzogranites are dominant medium-grained (1.0–3.5 mm) equigranular texture, containing scattered phenocrysts of alkali feldspar (5–20 mm long), composed of

Table 3
Summary of SHRIMP U–Pb zircon results for the monzogranite of the Las Cañadas granitic complex.

Grain spot	U (ppm)	Th (ppm)	Th/U	Pb* (ppm)	f_{206} %	Radiogenic ratios						ρ	Age (Ma)				
						$^{206}Pb/^{238}U$	±	$^{207}Pb/^{235}U$	±	$^{207}Pb/^{206}Pb$	±		$^{206}Pb/^{238}U$	±	$^{207}Pb/^{206}Pb$	±	% Disc
ANC-10017 Monzogranite																	
1.1	2281	389	0.17	142	0.43	0.0721	0.0009	0.5643	0.0135	0.0567	0.0012	0.505	449	5	481	46	7
2.1	8861	111	0.01	623	0.34	0.0816	0.0009	0.6384	0.0091	0.0567	0.0005	0.816	506	6	482	18	−5
2.2	232	7	0.03	18	0.31	0.0910	0.0012	0.7365	0.0223	0.0587	0.0016	0.432	561	7	557	60	−1
3.1*	1450	303	0.21	93	0.32	0.0742	0.0009	0.5756	0.0096	0.0563	0.0007	0.712	461	5	463	26	0
4.1	1561	325	0.21	112	0.07	0.0831	0.0010	0.6773	0.0095	0.0591	0.0004	0.841	514	6	572	17	10
5.1*	1979	293	0.15	127	0.59	0.0745	0.0009	0.5890	0.0114	0.0573	0.0009	0.608	463	5	504	34	8
6.1	2220	519	0.23	150	0.20	0.0782	0.0009	0.6153	0.0088	0.0571	0.0005	0.819	485	5	494	18	2
7.1*	1619	366	0.23	107	0.12	0.0770	0.0009	0.6025	0.0083	0.0568	0.0004	0.859	478	5	482	16	1
8.1*	1725	237	0.14	112	0.04	0.0759	0.0009	0.5945	0.0079	0.0568	0.0003	0.893	471	5	485	13	3
9.1	1718	160	0.09	127	1.69	0.0844	0.0010	0.6623	0.0351	0.0569	0.0029	0.228	523	6	487	114	−7
10.1	2093	641	0.31	140	0.12	0.0776	0.0009	0.6106	0.0083	0.0571	0.0004	0.869	482	5	494	15	3
11.1	358	210	0.59	23	0.38	0.0753	0.0010	0.5565	0.0142	0.0536	0.0012	0.496	468	6	353	50	−33
12.1*	1423	218	0.15	94	0.43	0.0768	0.0009	0.5941	0.0128	0.0561	0.0010	0.555	477	5	457	40	−4
13.1*	1473	347	0.24	96	0.17	0.0756	0.0009	0.5857	0.0088	0.0562	0.0005	0.788	470	5	461	21	−2
14.1*	3260	64	0.02	215	1.11	0.0759	0.0009	0.6018	0.0162	0.0575	0.0014	0.439	472	5	510	53	8
15.1	158	58	0.36	26	0.19	0.1934	0.0026	2.0779	0.0481	0.0779	0.0015	0.580	1140	14	1145	37	0
15.2	722	75	0.10	51	0.17	0.0818	0.0010	0.6562	0.0118	0.0582	0.0008	0.684	507	6	537	29	6
16.1	844	105	0.12	60	0.11	0.0833	0.0010	0.6642	0.0108	0.0578	0.0006	0.747	516	6	524	24	2
17.1	1788	451	0.25	122	0.30	0.0794	0.0009	0.6214	0.0106	0.0567	0.0007	0.701	493	6	482	27	−2
18.1*	1860	325	0.17	119	0.98	0.0738	0.0009	0.5829	0.0153	0.0573	0.0013	0.454	459	5	504	51	9
19.1*	2527	736	0.29	166	0.28	0.0763	0.0009	0.5908	0.0106	0.0562	0.0008	0.657	474	5	460	30	−3
20.1	191	151	0.79	12	0.80	0.0737	0.0011	0.5944	0.0132	0.0585	0.0010	0.652	458	7	548	37	16

Due to the high to very high-U of many grains, correction for common Pb was made using the measured.
Error in FC1 Reference zircon calibration was 0.72% for the analytical session (not included in above errors but required).
Uncertainties given at the 1σ level; f206% denotes the percentage of ^{206}Pb that is common Pb.
Asterisk (*) indicates data points used for Concordia age calculation.

(modal proportions %) Pl (38.6) + Qtz (20.3) + Kfs (30.6) + Bt (9.4), with Zrn + Ap as accessory minerals, and secondary muscovite.

The plagioclase compositions range from $Ab_{67.6}$ $An_{32.0}$ $Or_{0.4}$ (Na-rich andesine) to $Ab_{70.8}$ $An_{28.7}$ $Or_{0.5}$ (Ca-rich oligoclase, Table 1d). Plagioclase forms tabular crystals, varying from anhedral to euhedral, and shows polysynthetic twinning and continuous zoning with cores affected by sericite alteration. Some crystals display deformation twinning (twin gliding). Myrmekite is observed in contact with alkali feldspar. Quartz forms anhedral crystals showing prevalent undulose extinction and is evenly distributed. The alkali feldspar ($Ab_{4.8}$ $An_{0.3}$ $Or_{94.9}$, Table 1d) is microcline; it forms rectangular crystals with irregular contours, with cross-hatched twinning, perthitic texture, and small inclusions of euhedral plagioclase.

Biotite occurs as tabular, euhedral to subhedral crystals with light to dark brown pleochroism. Radioactive minerals occur as scarce inclusions with strongly pleochroic halos. Biotite in the monzogranites is chemically similar to that in the tonalites, but it is slightly more Fe-rich, with $Fe^{2+}/(Fe^{2+} + Mg)$ between 0.54 and 0.59 (Table 1e).

Muscovite is the other sheet silicate mineral present. Care was taken to determine whether it was primary or secondary in origin, since primary white mica is widely held to be an indicator of peraluminous magmas (Speer, 1984). Petrographic observations using the criteria of Miller et al. (1981) suggest that the muscovites (Table 1f) are of secondary origin (e.g., enclosure by any mineral from which the muscovite may have formed through alteration; Fig. 4b). Most primary muscovite are considerably richer in TiO_2, Al_2O_3 and NaO_2 and poorer in MgO (<1%) and SiO_2 (<45.5%) than secondary micas (data from Miller et al., 1981; Clarke et al., 2005; Dahlquist et al., 2007). Additionally, primary white micas are typically closer to ideal muscovite composition than their secondary counterparts, primarily because of lower MgO (Miller et al., 1981). White micas in the monzogranite of Las Cañadas complex have high MgO (1.48–1.53 wt.%) and SiO_2 (45.47–46.56 wt.%), strongly suggesting a secondary origin that is consistent with the petrographic criteria. Secondary epidote and muscovite are associated with biotite. Muscovite is also observed as a secondary mineral derived from plagioclase. Apatite occurs as prismatic and short crystals included in biotite and quartz.

6. Whole-rock geochemistry

6.1. Major and trace elements

The studied rocks of the Las Cañadas granitic complex display a wide compositional range albeit concentrated in two clusters (Table 2), SiO_2 varying from 61 wt.% (tonalite) to 73 wt.% (monzogranite). The granitic complex is metaluminous to slightly peraluminous with an alumina saturation index ranging from 1.06 for the tonalite to 1.14 for the monzogranite (using average values from Table 2), with agpaitic indices of 0.46 and 0.67, respectively. In the TAS diagram (Fig. 5) the samples define a typical calc-alkaline trend; compositions intermediate between tonalite and monzogranite (e.g., granodiorite) are apparently absent, but since basement rocks in the studied area are partially covered by vegetation and modern sediment, the possibility of unexposed intermediate rocks cannot not be dismissed. Harker variation diagrams (Fig. 6) display trends similar to those of other calc-alkaline granitoids (e.g., granitoids of the Sierra de Chepes, a classical calc-alkaline suite of the Famatinian magmatism, data in Dahlquist, 2002; Fig. 6). The biotite-bearing tonalites have higher CaO, Al_2O_3, Na_2O, FeO^t, MgO, TiO_2 and MnO concentrations, whereas the monzogranites have higher K_2O concentrations (Fig. 6).

Zr defines a steep negative trend (Fig. 7); concentrations of about 800 ppm in the calc-alkaline biotite-bearing tonalites (Table 2) are unusual. In the same way, these rocks have Zr/Hf ≈ 45, well above the chondritic value (Zr/Hf ≈ 37, Fig. 7) and close to the average Zr/Hf in zircon (Bea et al., 2006). These authors conclude that a higher-than-chondrite Zr/Hf value in a rock is caused by

Table 4
LA-ICP-MS zircon results for the biotite-bearing tonalite and monzogranite of the Las Cañadas complex.

Grain spot	$^{238}U/^{206}Pb$	1σ	rho	$^{207}Pb/^{206}Pb$	1σ	$^{206}Pb/^{238}U$ age	1σ	$^{207}Pb/^{206}Pb$ age	1σ	$^{207}Pb/^{206}Pb$	1σ	$^{207}Pb/^{235}U$ age	1σ
ANC-11030a Tonalite													
ANC-11030a_2a*	13.344	0.206	0.946	0.05601	0.00032	466	7	453	13	0.57873	0.02015	464	13
ANC-11030a_5a*	13.505	0.209	0.967	0.05608	0.00024	461	7	456	10	0.57254	0.01927	460	12
ANC-11030a_7a*	13.170	0.117	0.916	0.05638	0.00029	472	4	467	11	0.59025	0.01395	471	9
ANC-11030a_8a*	13.339	0.135	0.912	0.05744	0.00033	466	5	509	12	0.59378	0.01551	473	10
ANC-11030a_9a	12.828	0.111	0.916	0.05836	0.00030	484	4	543	11	0.62730	0.01453	494	9
ANC-11030a_24a*	13.209	0.118	0.897	0.05667	0.00034	470	4	479	13	1.46916	0.05116	472	21
ANC-11030a_25a*	13.432	0.068	0.915	0.05640	0.00031	463	2	468	12	0.59158	0.01479	464	9
ANC-11030a_1a	6.640	0.106	0.967	0.07075	0.00032	904	14	950	9	0.57898	0.01129	918	7
ANC-11030a_17a	11.720	0.082	0.890	0.05940	0.00035	528	4	582	13	0.69887	0.01554	538	9
ANC-11030a_18a	2.383	0.106	0.971	0.11516	0.00127	2258	84	1882	20	6.66208	0.62036	2068	79
ANC-11022 Monzogranite													
ANC-11022_1a	13.513	0.149	0.913	0.05720	0.00036	460	5	499	14	0.58363	0.01692	466.8	10.8
ANC-11022_4a	6.207	0.051	0.892	0.07265	0.00047	963	7	1004	13	1.61375	0.04052	975.6	15.6
ANC-11022_9a	2.877	0.023	0.926	0.11574	0.00060	1923	13	1892	9	5.54597	0.12904	1907.8	19.8
ANC-11022_10a	8.446	0.068	0.887	0.06418	0.00042	721	6	748	14	1.04760	0.02640	727.7	13.0
ANC-11022_XIIa	11.755	0.171	0.961	0.05838	0.00029	526	7	544	11	0.68474	0.02326	529.6	13.9

$^{238}U/^{206}Pb$ ratio corrected for static fractionation using FC1 for ANC-11030a and Peixe zircon standard ANC-11022.
Measurement errors represent within-run uncertainty only.
$^{207}Pb/^{206}Pb$ ratios corrected for static fractionation using FC1 for ANC-11030a and Peixe for ANC-11022.
Asterisk (*) indicates data points used for Concordia age calculation.

effective precipitation of zircon, which gives support to the idea that biotite-bearing tonalite have zircon 'cumulus'. On the other hand, the low Zr/Hf (Fig. 7) of the monzogranites supports progressive fractional crystallization with dominant fractionation of zircon.

6.2. Rare earth elements

Chondrite-normalized REE patterns of the two metaluminous facies of the Las Cañadas granitic complex (Fig. 8 and Table 2) are distinctively different. The tonalites have low LREE and high HREE values ($[La/Yb]_N = 5.22$), with marked positive Eu-anomalies ($Eu/Eu^* = 1.40$), strongly suggesting that they are adcumulates. Conversely, the monzogranites have negative Eu-anomalies ($Eu/Eu^* = 0.57$) and they are enriched in LREE and impoverished in HREE relative to the tonalites ($[La/Yb]_N = 11.48$).

7. Zircon saturation temperatures (T_{Zr})

Zircon saturation temperatures calculated from bulk-rock compositions using the equation of Miller et al. (2003) yield different temperatures of crystallization for each granitic facies (Table 2). Steep negative trends for both Zr and SiO_2 content together with T_{Zr} are defined by rocks of the Las Cañadas granitic complex (Fig. 9a,b), yielding T_{Zr} values ranging from 878° to 802 °C for the assumed parental magma equivalent to granodiorite composition and the differentiated monzogranitic magma, respectively (Table 2). These results are discussed in the Section 9.

8. Geochronology and Nd isotope geochemistry

As indicated in Section 4, the samples analysed in this work represent both granitic facies of the Las Cañadas granitic complex

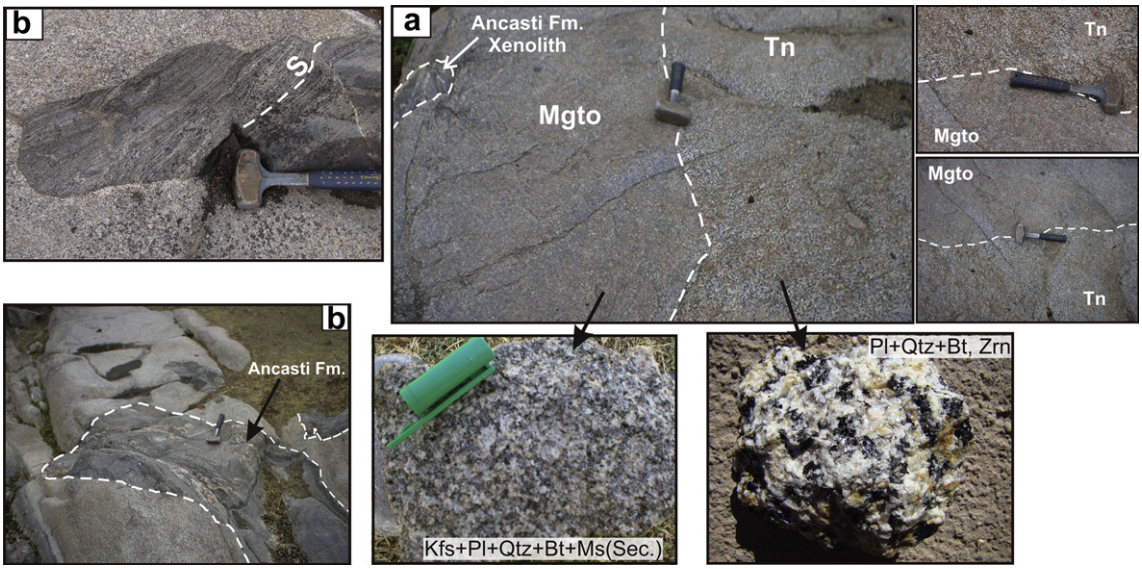

Fig. 3. Field characteristics of the Las Cañadas granitic complex at the San Francisco river. (a) Tonalite and monzogranite in outcrop, with hand samples. The mineral assemblages are shown on the photographs. The sharp contact between monzogranite and tonalite is also shown. (b) Metamorphic xenolith (Ancasti Formation) in monzogranite. 'S' is the metamorphic foliation.

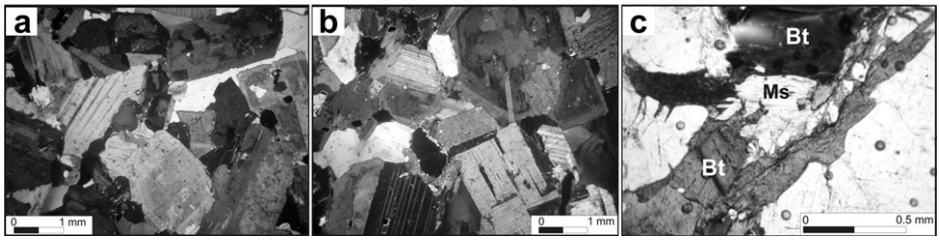

Fig. 4. Photomicrographs of typical minerals of the tonalite and monzogranite of the Las Cañadas granitic complex (ANC-11030, 11027, and 11022). (a) Polycrystalline adcumulate texture with cumulus plagioclase (ANC-11030). Similar samples were used in the mathematical model using major and trace elements. (b) Textural relation between muscovite and biotite strongly suggests that muscovite was formed through a *subsolidus* process (ANC-11022). This textural relationship is largely dominant in the monzogranite of the Las Cañadas granitic complex.

(Fig. 2 and Table 2): (i) ANC-10017 and ANC-11022 are typical monzogranites and (ii) ANC-11030a is a biotite-bearing tonalite (see Section 5.2.1).

8.1. Sample ANC-10017

The zircons from this sample are mostly elongate grains with subhedral to euhedral terminations. Cathodoluminescence (CL) images (Fig. 10a) reveal a complex internal structure with very dark, high-U rims or overgrowths on zoned low-U (light CL) cores. Some grains are dominated by the light-coloured zoned components, which are interpreted as an inherited older component; a single analysed core has an age of c. 1145 Ma, whereas the dark-CL, high-U grains have $^{206}Pb/^{238}U$ ages of 460–560 Ma, also suggesting partial inheritance. The main aim was to date the high-U rims as they are considered to relate to the time of granite formation. In these, the U content ranges up to c. 8900 ppm, with many areas having 1500–3000 ppm U, above the normal range of the U–Pb calibration on SHRIMP. However this high-U gives rise to highly radiogenic Pb, even for Ordovician time, so that the radiogenic $^{207}Pb/^{206}Pb$ ratios and ages are better constrained than usual for SHRIMP data on Phanerozoic zircons. The data are therefore presented as ^{204}Pb-corrected ratios and ages. It should be noted that the low Th/U ratios of the rims/overgrowths is due to the high U, and do not indicate metamorphic zircon growth. There is a wide range of calculated ages, up to 1100 Ma but the majority are reasonably concordant and cluster between 550 and 450 Ma (Table 3). Some of this spread must be due to partial inheritance of older zircon. Nine of the eleven youngest data (ignoring those for 11.1, which is discordant and 1.1, which with a $^{206}Pb/^{238}U$age of 449 ± 5 Ma has probably suffered slight loss of radiogenic Pb) yield a Concordia age (Ludwig, 2003) of 470 ± 6 Ma (95% confidence limits, including a further 0.7% uncertainty in the FC1 reference zircon analyses). This is considered the best estimate for the crystallization of the host monzogranite.

8.2. Sample ANC-11030a

The zircons from this tonalite sample are mostly elongate grains with subhedral to euhedral terminations. The SEM-CL images reveal a complex internal structure with light cores or small very dark cores (xenocrystic?) surrounded by a light core zone and dark rims. Some grains are dominated by the light-coloured zoned components, which are interpreted as a totally inherited older component.

The majority of the zircon ages are again concentrated around 470 Ma age and the age range of older inherited zircon is similar to that shown by the SHRIMP data for the monzogranite (Table 4). Six data points yield a Tera-Wasserburg Concordia age (Ludwig, 2003) of 466 ± 6 Ma (95% confidence limits, again allowing for the uncertainty in U/Pb calibration). This is considered the best estimate for the crystallization of the host tonalite (Fig. 10b). The range of ages from inherited zircon was expanded by the additional analyses of ANC-11022, another sample of monzogranite, as seen in Fig. 10b. Taking the SHRIMP data into account as well, inheritance ages of ~1900 Ma, ~900–1000 Ma, and 520–530 Ma are apparent with one grain noted at ~720 Ma.

8.3. Sm–Nd data of ANC-11030 and ANC-1022

The biotite-bearing tonalite and the monzogranite of the Las Cañadas granitic complex have similar $^{143}Nd/^{144}Nd$ ratios, 0.512212 and 0.512233, respectively. These rocks yield negative $\varepsilon_{Nd(t)}$ values of −3.3 and −5.0 and T_{DM} ages of 1.5 and 1.6 Ga (Table 5); these are typical values observed in the metaluminous granitic rocks of the Famatinian magmatism that were derived from the partial melting of old continental lithosphere (e.g., Pankhurst et al., 1998, 2000; Dahlquist et al., 2008 and references therein). Typical S-type Famatinian granites have $\varepsilon_{Nd(t)}$ values ranging from −5.0 to −6.7 (Pankhurst et al., 1998; Dahlquist et al., 2007).

9. Petrogenetic model

In order to define the main differentiation process during the crystallization, we have assessed two mathematical models as discussed below.

9.1. Fractional crystallization model based on major oxides

On the basis of the preceding observations it was considered that the main mechanism of differentiation was fractional

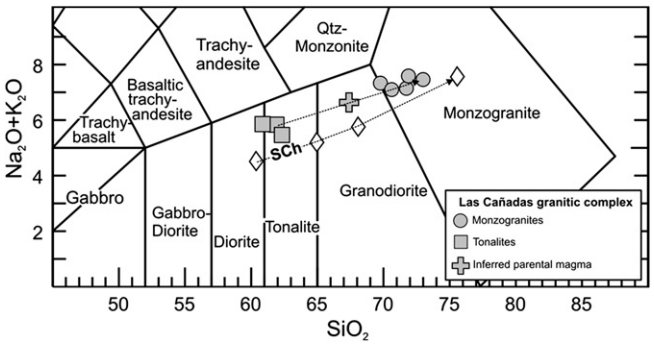

Fig. 5. Granitoids plotted in the TAS diagram (Middlemost, 1994) showing dominant tonalitic and monzogranitic compositions in the Las Cañadas granitic complex. A theoretical granodiorite composition (filled cross) calculated from the fractional crystallization model is shown in this figure and explained in the Section 9. SCh = Sierra de Chepes calc-alkaline metaluminous trend (open diamonds) using average values from Dahlquist et al. (2006), including mafic microgranular enclave, tonalite, granodiorite, porphyritic granodiorite, and monzogranite compositions, respectively.

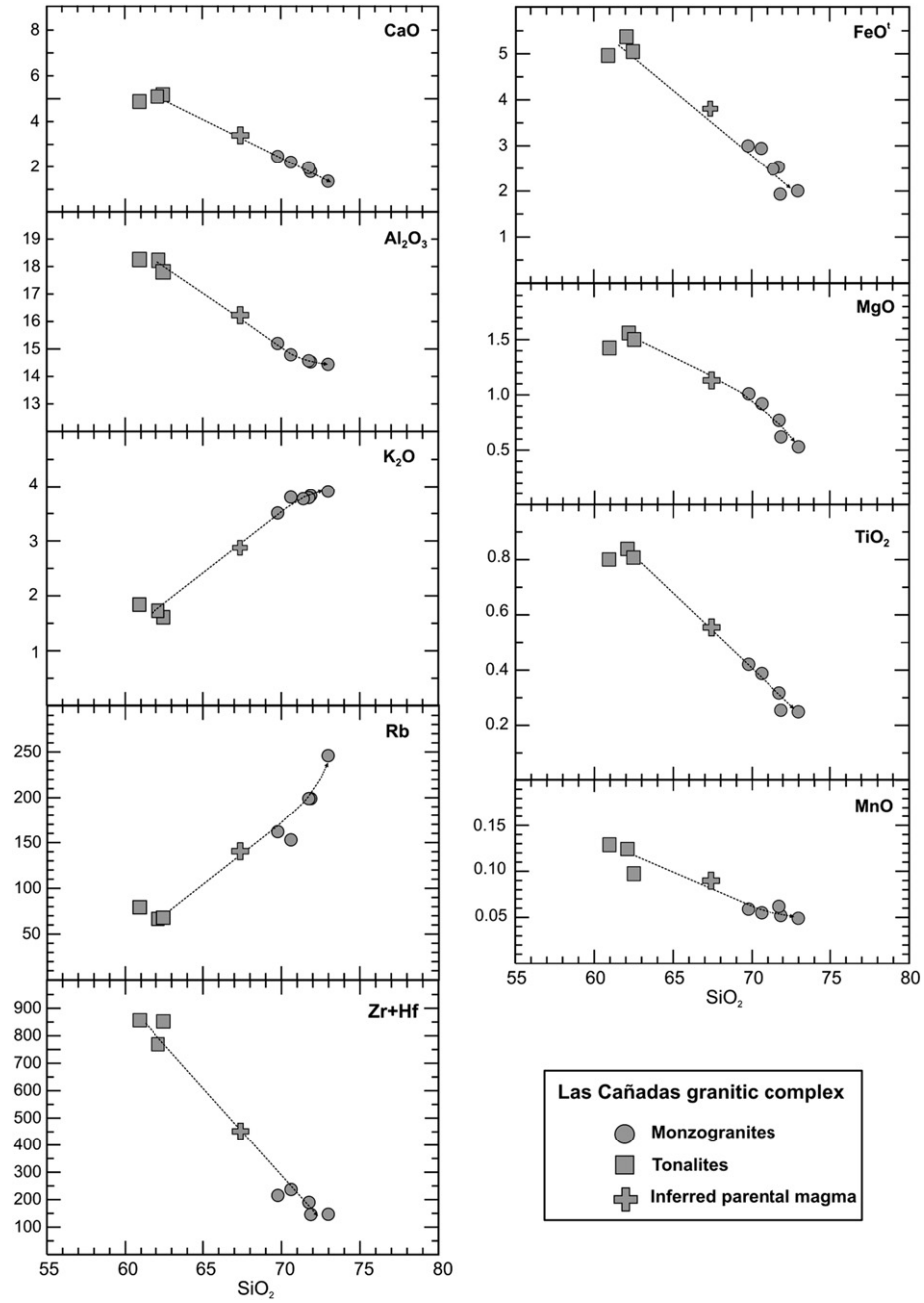

Fig. 6. Harker variation diagrams showing the main trends (discontinuous line) defined by the observed end-member compositions, tonalite and monzogranite in the Las Cañadas granitic complex. A theoretical granodiorite composition (filled cross) calculated from the fractional crystallization model is shown in this figure and explained in the Section 9.

crystallization in a nearly closed system. Samples used in the fractional crystallization model were selected based on both textural features and whole-rock geochemistry. Thus, an average composition of the tonalites with biotite as the only mafic mineral, was assumed to represent the most typical early crystallization product, whereas an average composition of the monzogranites was taken as the most typical resultant evolved melt (data in Table 2); the parental magma from which tonalitic rocks accumulated to produce the differentiated of monzogranitic compositions magma was considered as being composed of 45% of the former and 55% of the latter. Rocks corresponding to the parental magma do not appear in outcrop, but this may have been effectively consumed by extreme fractionation; the latter explanation was preferred by Johannes et al. (2003) and Dahlquist et al. (2007) in fractional crystallization models for granitic rocks. A 45:55 mixture is the best-fit model estimate of the parental magma (Table 2). The used mineral chemical was that reported for ANC-11030 in Table 1. Least-square regression methods for modelling the segregation of crystallizing minerals (Bryan et al., 1969; Walker and Carr, 1986) were performed using IGPET (Carr, 1998). Details of the calculations and the results are shown in Table 6. The fractional crystallization calculation shows a very acceptable ΣR^2 value (= sum of the squares of the residuals) for plutonic rocks (Dahlquist, 2002; Gomes and Neiva, 2005; Dahlquist et al., 2007), and the calculated modal value of the early crystallized cumulate is similar to that of ANC-11030 (Table 6). Nevertheless, the natural variables involved during magma crystallization in plutonic systems mean that the numerical results of modelling (e.g., relative percentages of

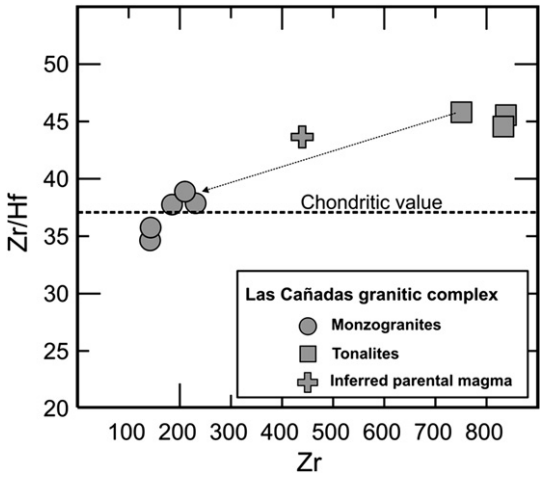

Fig. 7. Zr/Hf concentration in the rocks of the Las Cañadas granitic complex. The chondritic ratio of 37.1 is from Bea et al. (2006). The tonalites and monzogranites are strongly enriched and depleted in Zr/Hf ratios, respectively.

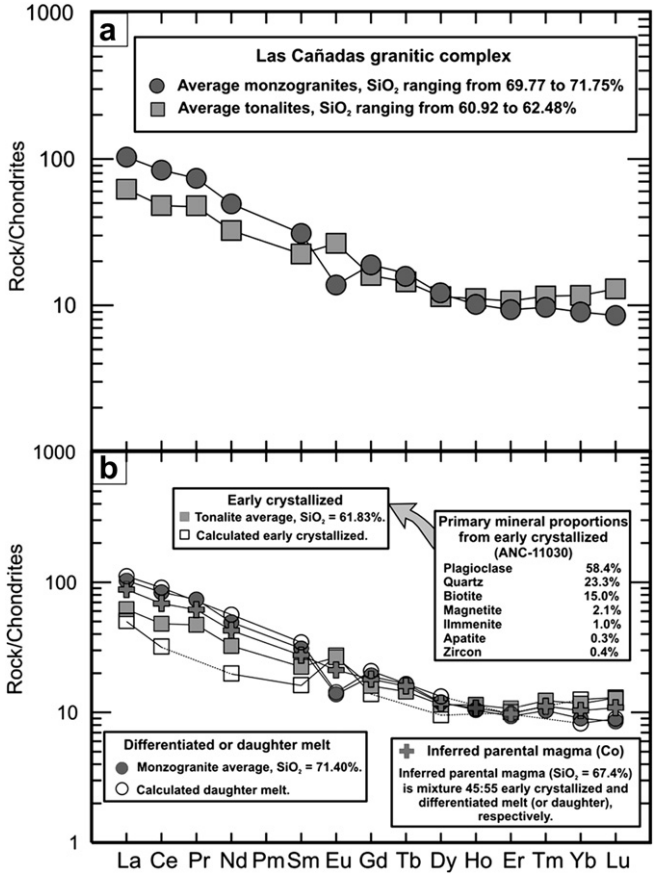

Fig. 8. Chondrite-normalized rare earth element patterns for the Las Cañadas granitic complex. (a) Average REE patterns of tonalite and monzogranite displaying low LREE and high HREE values, with marked positive Eu-anomalies. Conversely, the monzogranites have negative Eu-anomalies and they are enriched in LREE and impoverished in HREE content with regard to the tonalities, suggesting a genetic relationship. (b) Average REE patterns of tonalite and monzogranite together with the results from the fractional crystallization model which is shown in this figure and explained in the text (data in Table 6). The close agreement between observed and calculated patterns supports a fractional crystallization process. Chondrite concentrations according to Nakamura (1974); Tb, Ho, and Tm are according to Boynton (1984).

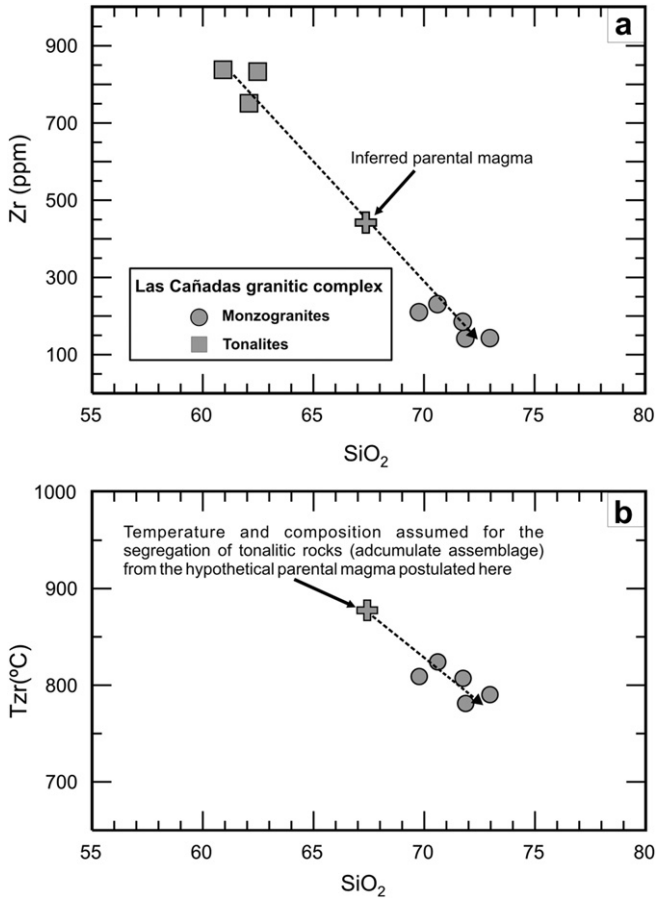

Fig. 9. (a) Zr–SiO_2 variation diagram and (b) plot of T_{Zr} versus SiO_2 for the La Cañada granitic complex (I-type granites). The steep decrease in Zr content and T_{Zr}, with evolution to higher silica (from tonalite to monzogranite composition) is compatible with zircon separation. The inferred parental magma composition was calculated in Section 9 and the data are shown in Tables 2, 5, and 6.

fractionating minerals) should be taken as no more than approximations to reality.

9.2. Fractional crystallization model based on trace elements

The same samples were also used for a trace element fractional crystallization model assuming the same composition of the parental magma (a 45:55 mix between tonalite and monzogranite average), using the approach of Hanson (1978). The concentration of any trace element 'i' in the differentiated melt (C_L^i) relative to that in the parent melt (Co) during fractional crystallization is given by the Rayleigh fractionation law: $C_L^i = C_o^i \cdot F^{(D-1)}$ where F is the fraction of melt remaining and D is the bulk distribution coefficient of the fractionating assemblage, given by $D = \Sigma X^i \cdot K^i$, where X^i is the modal proportion of each mineral, and $K^{i/l}$ is its mineral–melt partition coefficient. F = 0.65 as well as the initial concentration of REE elements (C_o^i) were chosen from the results obtained in the previous section and are shown in Table 6. Modal proportions X^i are those previously obtained from the fractional crystallization model based on major oxides (Table 7). K^i was assumed to be constant during the crystallization process; the values used and other details are founded in Table 7. There is a close correspondence between the observed and calculated values of C_L^i (differentiated melt), as is evident in Fig. 8b.

The REE reside mostly in accessory minerals, where they are essential structural components, and Henry's law is not applicable.

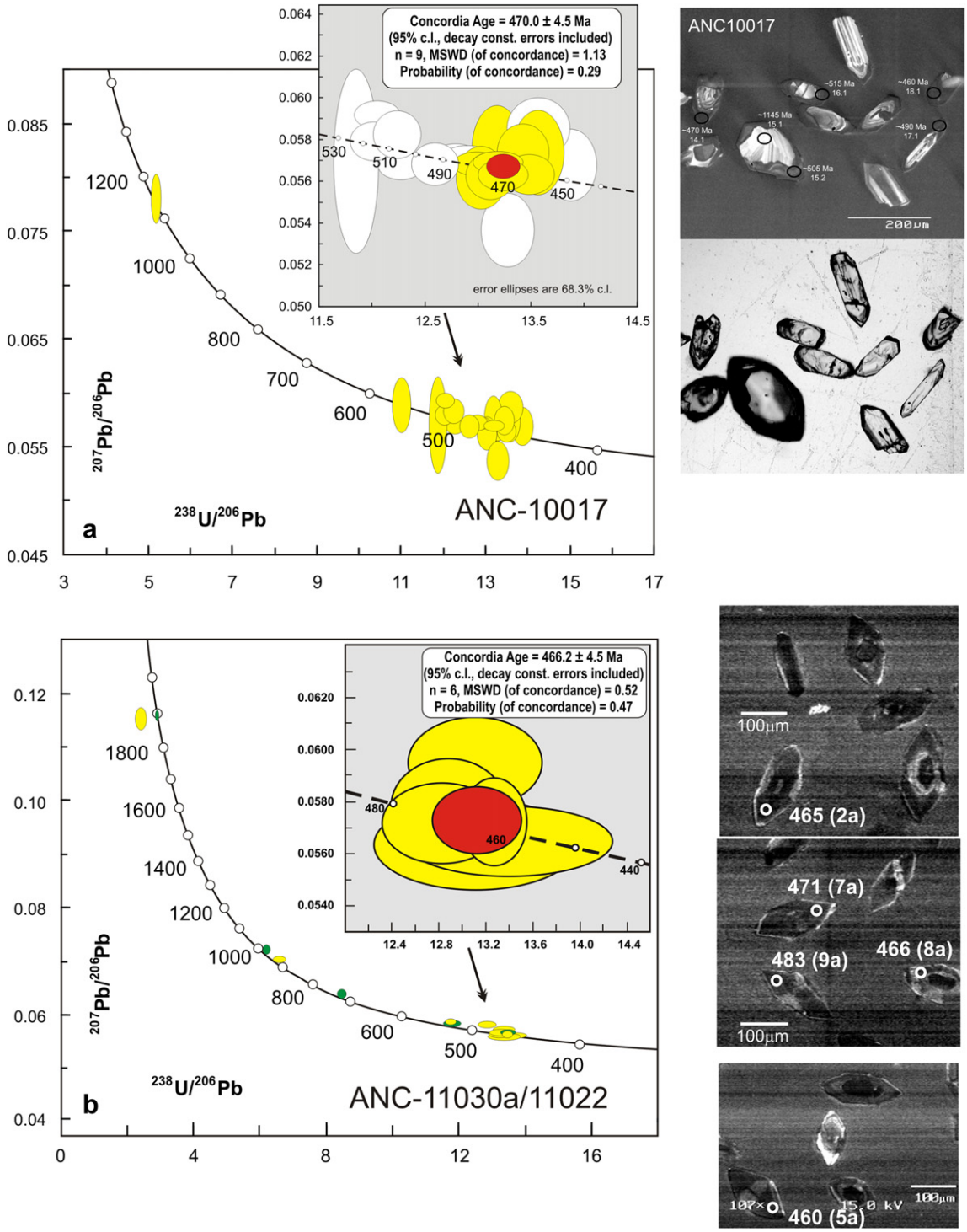

Fig. 10. U–Pb zircon dating of the Las Cañadas granitic complex. (a) U–Pb SHRIMP data for monzogranite ANC-10017, showing transmitted-light and CL images for the same portion of the mount, and a Tera-Wasserburg plot showing a majority of the analyses plotting between 450 and 550 Ma. The older ages are thought to represent retained inheritance, as clearly indicated by the zoned core of grain #15 which gave an age of 1145 Ma. The main group of analyses for the high-U rims give a Concordia age of 470 ± 5 Ma (inset), but the uncertainty expands to ± 6 Ma taking the U/Pb calibration uncertainty into account. (b) U–Pb LA-ICP-MS results for tonalite ANC-11030a, showing SEM-CL images for the same portion of the mount. The main Tera-Wasserburg plot shows all analyses from this sample and monzonite ANC-11022 (green), demonstrating a similar inheritance range to ANC-11030a (yellow). Most analyses plotting between 460 and 480 Ma and the inset shows a Concordia age of 466 ± 5 Ma for this subgroup (similarly expanded to ± 6 Ma when the calibration uncertainty is added). (For interpretation of the references to colour in this figure legend, the reader is referred to the web version of this article.)

Thus, granitic rocks with significant accessory minerals are not generally suitable for calculations based on a Rayleigh fractionation model (Bea, 1996). In the present case we assume that Rayleigh fractionation applied during differentiation because: (i) accessory minerals (with exception of zircon and apatite, which have less effect on REE contents) were not recognized in the biotite-bearing tonalite, (ii) the relatively low REE concentration in the tonalite is not consistent with the effective crystallization of accessory

Table 5
Sm–Nd isotopic compositions.

Samples	SiO_2 (*wt. %*)	Age (Ma)	Sm (*ppm*)	Nd (*ppm*)	$^{147}Sm/^{144}Nd$	$(^{143}Nd/^{144}Nd)_0$	$(^{143}Nd/^{144}Nd)_t$	$\varepsilon_{Nd(t)}$	T_{DM}^* (Ga)
ANC-11030a	60.92	466	3.914	16.766	0.1412	0.512212	0.511779	−5.0	1.6
ANC-11022	71.75	470	5.984	30.198	0.1198	0.512233	0.511863	−3.3	1.5

The ^{147}Sm decay constant used in the calculations is 6.54×10^{-12} year^{-1} (Steiger and Jaëger, 1977). Epsilon Nd (ε_{Nd}) values were calculated relative to a chondrite present day: $(^{143}Nd/^{144}Nd)^{today}_{CHUR} = 0.512638$; $(^{143}Sm/^{144}Nd)^{today}_{CHUR} = 0.1967$. t = time used for the calculation of the isotopic initial ratios. T_{DM}^* = calculated according to DePaolo et al. (1991).

minerals (Dahlquist, 2001), (iii) fractional crystallization models using major oxides (in which accessory minerals do not participate) and trace elements are both consistent with tonalite being an adcumulate assemblage and monzogranite a differentiated melt, each derived from the hypothetical parental magma postulated here. This evidence supports the hypothesis that fractional crystallization was the main differentiation process in the Las Cañadas granitic complex.

10. Discussion: petrogenesis of the Las Cañadas granitic complex

The REE patterns of tonalite and monzogranite are distinct, as noted above. The monzogranites are enriched in LREE and impoverished in HREE, with negative Eu-anomalies whereas, in comparison, the tonalites are impoverished in LREE and enriched in HREE and show a marked positive Eu-anomaly (Fig. 8a,b). These rocks can thus be considered a differentiated melt and early crystallized, respectively.

The chemical signature of REE and the fractional crystallization models presented above (using major and trace element) are fully consistent with a fractional crystallization process, with a parental magma represented by a mixture of 45% tonalite and 55% monzogranite, and where tonalite and monzogranite are early crystallized cumulate and differentiated melt, respectively (Fig. 8b). Thus, the abundant patchy zoning in plagioclase in the tonalite samples (see Section 5.2.1.) is interpreted as due to resorption of early crystals and infilling of the corroded regions by more sodic material (Vance, 1962; Anderson, 1984). This is consistent (together with the field evidence and chemical data considered in the previous section) with the assumption that the tonalite is an older, plagioclase-rich facies, segregated early from the inferred parental magma and reheated during intrusion of later monzogranite facies. Similar petrographic characteristics have been observed in plagioclase crystallized in segregates of tonalite composition (Dahlquist et al., 2007) and with distinctive plagioclase enrichment (~64%, modal proportion).

The occurrence of inherited cores in zircons in the studied sample (monzogranite ANC-10017, ANC-11022, and ANC-11030a) suggests that zircon may have come from sediment weathered from an igneous source or they may have come directly from melting of an igneous source with different ages. A mixed igneous and sedimentary source for granitoids of metaluminous composition has been widely reported in the Lachlan Fold Belt (southeastern Australia) by Chappell and White (1992), Chappell (1996, 1997), and Kemp et al. (2005 and references therein). In particular, Chappell (1997) and Kemp et al. (2005) indicate that mixing of components may still be a viable model for the generation of parental metaluminous magmas that later fractionated in some way (e.g., by fractional crystallization) to produce the compositional variation observed within suites. In our study, further systematic dating of inherited zircon cores would be required to clarify this topic.

The initial $^{143}Nd/^{144}Nd$ ratios (−3.3 and −5.0) and T_{DM} (1.5 and 1.6 Ga) calculated to 470 and 466 Ma, respectively, indicate that the parental magma was principally derived from partial melting of old continental crust. The inherited core zircons indicate the residue of an evolved crustal component in the metaluminous granitic magma of the Las Cañadas granitic complex. These results for one of the easternmost outcrops of the Famatinian arc are consistent with studies carried out in other areas of the Sierras Pampeanas further west, which confirm that the Famatinian magmatic belt was short-lived (~20 Ma) and without a significant asthenospheric contribution (see previous isotopic data reported by Pankhurst et al.,

Table 6
Results of fractional crystallization model for the Las Cañadas granitic complex.

Calculated extracted phases in the early crystallized (modal %)	Compositions mineral utilized in the calculation (ANC-11030)[a]	Modal values from ANC-11030[b]
58.4	Plagioclase (An_{43})	Plagioclase = 61.2%.
23.3	Quartz (SiO_2)	Quartz = 21.2%.
15.0	Biotite [$Fe^{2+}/(Fe^{2+} + Mg) = 0.55$]	Biotite = 14.2%.
2.1	Magnetite ($Fe_2O_3 = 98.53\%$)	Magnetite*.
1.0	Ilmenite ($TiO_2 = 47.7\%$)	Ilmenite*.
0.3	Apatite ($F = 4.65\%$)	Apatite = nmd.

Weight fractions (%) of magma remaining with a composition equal to ANC-11022 (daughter magma) = 59.80

	SiO_2	TiO_2	Al_2O_3	FeO^t	MnO	MgO	CaO	Na_2O	K_2O	P_2O_5
Daughter magma[c]	72.23	0.32	14.67	2.55	0.06	0.78	1.97	3.36	3.82	0.25
Parental magma[c]	67.40	0.55	16.19	3.80	0.09	1.12	3.37	3.67	2.86	0.27
Determined parental magma	67.86	0.55	16.30	3.83	0.09	1.13	3.39	3.69	2.88	0.27
Calculated parental magma	67.86	0.55	16.31	3.83	0.09	1.07	3.45	3.62	2.93	0.20
Difference obs.-calc. $\Sigma R^2 = 0.020$	0.00	0.00	−0.02	0.00	0.00	0.06	−0.06	0.07	−0.05	0.07

Whole-rock chemistry data in Table 2. Determined and calculated parental magma compositions were obtained using IGPET program (Carr, 1998). This program makes fractional crystallization calculations using least-squares regression of the major elements, after Bryan et al. (1969).
Abbreviations: nmd = no modal data. ΣR^2 = sum of the squares of the residuals.
*Modal data of 1.13% represent magnetite + ilmenite.
[a] Mineral chemistry in Table 1. Plagioclase and biotite are an average from Tables 1a and 1b.
[b] Modal proportions of ANC-11030 in the text.
[c] Daughter magma is ANC-11022 and the parental magma is derived from simple mixing of early crystallized (45% ANC-11030) and daughter magma (55%, ANC-11022).

Table 7
Data used in the fractional crystallization mathematical model for the Las Cañadas granitic complex.

Minerals[a]	Modal proportion for early crystallized	$Kd^{S/L}$ (La)	$Kd^{S/L}$ (Ce)	$Kd^{S/L}$ (Nd)	$Kd^{S/L}$ (Sm)	$Kd^{S/L}$ (Eu)	$Kd^{S/L}$ (Gd)	$Kd^{S/L}$ (Dy)	$Kd^{S/L}$ (Er)	$Kd^{S/L}$ (Yb)	$Kd^{S/L}$ (Lu)
Pl	58.4	0.490[b]	0.251[g]	0.189[b]	0.1366[h]	2.81[m]	0.90[p]	0.452[i]	0.242[q]	0.302[n]	0.062[i]
Qtz[c]	23.3	0.018	0.014	0.016	0.017	0.080	0.018	0.017	0.018	0.017	0.011
Bt	15.0	0.318[d]	0.377[d]	0.044[i]	0.390[d]	1.080[o]	0.280[p]	0.097[q]	0.162[q]	0.440[m]	0.33[m]
Mag	2.1	0.450[e]	0.420[e]	0.930[j]	0.074[l]	0.025[o]	0.018[i]	0.58[q]	0.017[t]	0.11[l]	0.38[e]
Ilm[f]	1.0	0.015	0.110	0.010	0.009	0.010	0.140	0.140[s]	0.067	0.170	0.190
Ap	0.3	28.2[g]	37.4[g]	61.2[g]	98.5[g]	25.5[g]	21.7[n]	69.2[k]	80[k]	25[k]	7.9[n]
Zrn	0.4	4.18[g]	5.14[g]	6.51[k]	6.50[m]	3.10[h]	6.59[g]	53.5[k]	152[k]	299[k]	333[g]
		La	Ce	Nd	Sm	Eu	Gd	Dy	Er	Yb	Lu
C_o^i		29.00	59.36	6.89	26.86	5.57	1.63	4.03	2.20	2.27	0.37
Results obtained from the fractional crystallization mathematical model C_L^i (concentration in ppm)											
		La	Ce	Nd	Sm	Eu	Gd	Dy	Er	Yb	Lu
Observed Liquid O_L^i REE		35.70	74.70	31.90	6.33	1.08	5.16	3.72	1.77	1.71	0.252
Calculated Liquid C_L^i REE		36.91	74.01	31.06	6.38	1.03	5.43	3.81	1.78	1.70	0.298
Observed Solid O_S^i REE		20.80	40.60	20.70	4.65	2.96	4.73	4.40	2.73	2.96	0.514
Calculated Solid C_S^i REE		16.22	36.11	20.58	4.39	2.13	4.30	4.31	2.66	2.84	0.448

Equation describing fractional crystallization is the equation for Rayleigh fractionation: $C_L^i = C_o^i \cdot F^{(D-1)}$.
C_o^i: the weight concentration in the parental melt is a mixing from 55% early crystallized (average tonalites) and 45% of fractionated melt (average monzogranites). Data in Tables 2 and 6.
D^i = Bulk distribution coefficient of the fractionating assemblage during crystal fractionation = $\Sigma X^i \times Kd^{S/L}$; where X^i is the mineral proportion crystallizing from the parental liquid and $Kd^{S/L}$ is the solid–liquid partition coefficient of phase i. X^i = calculated modal proportions in Table 6.
F = weight fraction of melt produced in fractional crystallization. $F = 0.65$.
O_L^i = Average Monzogranite. Data in Table 2.
O_S^i = Average Tonalite. Data in Table 2.
C_L^i = weight concentration of a trace element "i" in the calculated fractionated melt.
C_S^i = weight concentration of a trace element "i" in calculated early crystallized.
[r]Luhr and Carmichael (1980).
[a] Proportion minerals from calculated extracted phases in Table 6. Mineral proportion of Zrn = 0.04 is assumed, using those yields the best fit in the fractional crystallization model.
[b] Dudas et al. (1971).
[c] Nash and Crecraft (1985).
[d] Matsui et al. (1977).
[e] Beattie (1993).
[f] Jang and Naslund (2003).
[g] Fujimaki (1986).
[h] Fujimaki et al. (1984).
[i] Schnetzler and Philpotts (1970).
[j] Bacon and Druitt (1988).
[k] Nagasawa (1970).
[l] Sisson (1991).
[m] Higuchi and Nagasawa (1969).
[n] Nagasawa and Schnetzler (1971).
[o] Villemant et al. (1981).
[p] Arth (1976).
[q] Paster et al. (1974).
[s] Kd for Dy is from an average using Kd Gd and Tb.
[t] Kd for Er is from an average using Kd Ho. Mineral abbreviations from Kretz (1983)

1998, 2000; Rapela, 2000; Dahlquist and Galindo, 2004; Dahlquist et al., 2007, 2008), in contrast to the long-lived (~200 Ma) cordilleran magmatism of the Andes with direct asthenospheric participation (e.g., Parada et al., 1999; Dahlquist and Galindo, 2004; Dahlquist et al., 2008). Fractional crystallization has been reported in other intrusive complexes of the Famatinian arc, and seems to be a common differentiation process for these granitic rocks (e.g., Dahlquist, 2002; Dahlquist et al., 2007).

The steep decrease in Zr content and T_{Zr} with evolution to higher silica (from tonalite to monzogranite composition) is compatible with progressive zircon crystallization (Figs. 7 and 9a,b and Table 2) leading to a differentiated melt and an early crystallized adcumulate with low and very high Zr contents, respectively (Fig. 9a). Therefore, we conclude that the geochemical data (Section 6 and 9) and the steep negative trends for the Zr content and T_{Zr} are consistent and strongly support a fractional crystallization process. Using the parental magma composition calculated in Section 9 and the calculated T_{Zr} (Table 2), we conclude that the onset of zircon crystallization (together with other crystallizing phases) occurred when the parental magma reached ~67 wt.% SiO_2 and ~440 ppm of Zr at ~878 °C (Fig. 9 and Tables 2, 6, and 7). These values are very similar to those reported for the onset of zircon crystallization in granitic rocks of metaluminous composition outcropping in the Lachlan Fold Belt, SW of Australia: 65 wt.% SiO_2 and 460 ppm of Zr at ~870 °C (Kemp et al., 2005).

11. Conclusions

Ordovician granitoids of the Las Cañadas complex were emplaced in continental crustal host rocks at close to 468 Ma (the crystallization ages of 470 ± 6 and 466 ± 6 Ma determined here for monzogranite and tonalite respectively by independent U–Pb analytical methods cannot be distinguished at the level of analytical precision). All available data, including field and petrographic relationships, mineral chemistry, bulk major and trace element compositions, support a model of differentiation by fractional crystallization for the calc-alkaline metaluminous rocks of the Las Cañadas granitic complex.

The presence of inherited zircon cores in the metaluminous granites of the Las Cañadas granitic complex together with Nd–Sm isotopic data indicates that the parental magma was largely derived from partial melting of old continental lithosphere formed by (i) mixed igneous and sedimentary source or (ii) directly by igneous source with different ages. Independently of the source rock, the derived parental magma evolved by fractional crystallization. The onset of zircon crystallization together with variable amounts of other minerals such as Pl + Qtz + Bt + Oxides ± Ap occurred when the parental magma reached 67 wt.% SiO_2 and 440 ppm of Zr at ~878 °C.

The crystallization sequence has three main components, represented by the tonalite, monzogranite, and the inferred parental magma of granodioritic composition, where the tonalite represents plagioclase-rich early segregates and monzogranite a differentiated melt. Representative mineral assemblages are plagioclase and subordinate quartz and biotite in the tonalite, and plagioclase, quartz, biotite, and conspicuous alkali feldspar in the monzogranite.

Previous work (reported in Section 2) on the Famatinian magmatism indicates that it was largely derived from old continental crust and that fractional crystallization was a common differentiation process. The new data reported here are consistent with this scenario.

Acknowledgements

Financial support was provided by BID 1728 AR PICT 1009 (FONCyT), CGL2009-07984/BTE (Spain), SECyT-UNC 10/11, and a CONICET external fellowship awarded to Dr. Juan A. Dahlquist for his research stay at Washington State University. Juan A. Dahlquist thanks Dr. Rich Gaschnig (WSU) for comments on the manuscript and assistance with data as well as to Scotty Cornelius and Charles Knaack for their assistance with use of the electron microprobe and LA-ICP-MS, respectively. The careful and thorough reviews by one anonymous journal reviewer and the Professor David Chew improved the final form of the manuscript. Juan A. Dahlquist thanks to Alejandra all her love at this time.

References

Aceñolaza, F.G., Miller, H., Toselli, A.J., 1996. Geología del Sistema de Famatina. 19(6). In: Aceñolaza, F.G., Miller, H., Toselli, A.J. (Eds.), Geología del Sistema de Famatina. Münchner Geologische Hefte, Reihe A, p. 412.

Aceñolaza, F.G., Toselli, A.J., 1977. Esquema geológico de la sierra de Ancasti, provincia de Catamarca. Acta Geológica Lilloana 14, 233–256.

Anderson, A.T., 1984. Probable relations between plagioclase zoning and magma dynamics, Fuego Volcano Guatemala. American Mineralogist 69, 660–676.

Armstrong, J.T., 1988. Quantitative analysis of silicates and oxide minerals: comparison of Monte-Carlo, ZAF and Phi-Rho-Z procedures. In: Newbury, D.E. (Ed.), Microbeam Analysis. San Francisco Press, California, pp. 239–246.

Arth, J.G., 1976. Behavior of trace elements during magmatic processes — a summary of theoretical models and their applications. Journal of Research of the Geological Survey 4, 41–47.

Bacon, C.R., Druitt, T.H., 1988. Compositional evolution of the zoned calcalkaline magma chamber of Mount-Mazama, Crater Lake, Oregon. Contributions to Mineralogy and Petrology 98, 224–256.

Bea, F., 1996. Residence of REE, Y, Th and U in granites and crustal protoliths; implications for the chemistry of crustal melts. Journal of Petrology 37, 521–552.

Bea, F., Montero, P., Ortega, M., 2006. A LA-ICP-MS evaluation of Zr reservoirs in common crustal rocks: implications for Zr and Hf geochemistry, and zircon-forming processes. Canadian Mineralogist 44, 693–714.

Beattie, P., 1993. The effect of partial melting of spinel peridotite on uranium series disequilibria: constraints from partitioning studies. Earth and Planetary Science Letters 177, 379–391.

Bouvier, A., Vervoort, J.D., Patchett, J.P., 2008. The Lu–Hf and Sm–Nd isotopic composition of CHUR: constraints from unequilibrated chondrites and implications for the bulk composition of terrestrial planets. Earth and Planetary Science Letters 273, 48–57.

Boynton, W.V., 1984. Geochemistry of the rare earth elements: meteorite studies. In: Henderson, P. (Ed.), Rare Earth Element Geochemistry. Elsevier, Amsterdam, pp. 63–114.

Bryan, W.B., Finger, L.W., Chayes, F., 1969. Estimating proportions in petrographic mixing equations by least-squares approximation. Science 163, 926–927.

Büttner, S.H., Glodny, J., Lucassen, F., Wemmer, K., Erdmann, S., Handler, R., Franz, G., 2005. Ordovician metamorphism and plutonism in the Sierra de Quilmes metamorphic complex: implications for the tectonic setting of the northern Sierras Pampeanas (NW Argentina). Lithos 83, 143–181.

Carr, M.J., 1998. IgPet32 Program. Terra Software Inc.

Chang, Z., Vervoort, J.D., McClelland, W.C., Knaack, C., 2006. U–Pb dating of zircon by LA-ICP-MS. Geochemistry, Geophysics, Geosystems 7, 1–14. Q05009.

Chappell, B.W., White, A.J.R., 1992. I- and S-type granites in the Lachlan Fold Belt. Transactions of the Royal Society of Edinburgh: Earth Sciences 83, 1–26.

Chappell, B.W., 1996. Magma mixing and the production of compositional variation within granite suites: evidence from the granites of southeastern Australia. Journal of Petrology 37, 449–470.

Chappell, B.W., 1997. Compositional variation within granite suites of the Lachlan Fold Belt: its causes and implications for the physical state of granite magma. Transactions of the Royal Society of Edinburgh: Earth Sciences 88, 159–170.

Cisterna, C., 2003. Faja intrusiva La Majada, sierra de Ancasti, Catamarca: Caracterización petrológica-estructural. Revista de la Asociación Geológica Argentina 58, 20–30.

Clarke, D.B., Dorais, M., Barbarin, B., Barker, D., Cesare, B., Clarke, G., el Baghdadi, M., Erdmann, S., Förster, H.J., Gaeta, M., Gottesmann, B., Jamieson, A., Kontak, D.J., Koller, F., Gomes, C.L., London, D., Morgan VI, G.B., Neves, L.J.P.F., Pattison, D.R.M., Pereira, A.J.S.C., Pichavant, M., Rapela, C.W., Renno, A.D., Richards, S., Roberts, M., Rottura, A., Saavedra, J., Sial, A.N., Toselli, A.J., Ugidos, J.M., Uher, P., Villaseca, C., Visonà, D., Whitney, D.L., Williamson, B., Woodard, H.H., 2005. Occurrence and origin of andalusite in peraluminous felsic igneous rocks. Journal of Petrology 46, 441–472.

Dahlquist, J.A., 2001. REE fractionation by accessory minerals in epidote-bearing metaluminous granitoids from the Sierras Pampeanas, Argentina. Mineralogical Magazine 65, 463–475.

Dahlquist, J.A., 2002. Mafic microgranular enclaves: early segregation from metaluminous magma (Sierra de Chepes), Pampean Ranges, NW Argentina. Journal of South American Earth Sciences 15, 643–655.

Dahlquist, J.A., Alasino, P.H., Eby, G.N., Galindo, C., Casquet, C., 2010. Fault controlled Carboniferous A-type magmatism in the proto-Andean foreland (Sierras Pampeanas, Argentina): geochemical constraints and petrogenesis. Lithos 115, 65–81.

Dahlquist, J.A., Alasino, P.H., Galindo, C., Pankhurst, R.J., Rapela, C.W., Saavedra, J., Casquet, C., Baldo, E., González Casado, J.M., 2006. Evolución magmática del granito Peñón Rosado, cerro Asperecito, flanco occidental de la sierra de Famatina. Revista de la Asociación Geológica Argentina 61, 93–111.

Dahlquist, J.A., Galindo, C., 2004. Geoquímica isotópica de los granitoides de la sierra de Chepes: un modelo geotectónico y termal, implicancias para el orógeno famatiniano. Revista de la Asociación Geológica Argentina 59, 57–69.

Dahlquist, J.A., Galindo, C., Pankhurst, R.J., Rapela, C.W., Alasino, P.H., Saavedra, J., Fanning, C.M., 2007. Magmatic evolution of the Peñón Rosado granite: petrogenesis of garnet-bearing granitoids. Lithos 95, 177–207.

Dahlquist, J.A., Pankhurst, R.J., Rapela, C.W., Galindo, C., Alasino, P., Fanning, C.M., Saavedra, J., Baldo, E., 2008. New SHRIMP U–Pb data from the Famatina complex: constraining early–mid Ordovician Famatinian magmatism in the sierras Pampeanas, Argentina. Geologica Acta 6, 319–333.

Dahlquist, J.A., Rapela, C.W., Baldo, E.G., 2005. Cordierite-bearing S-type granitoids in the Sierra de Chepes (Sierras Pampeanas): petrogenetic implications. Journal of South American Earth Sciences 20, 231–251.

Dahlquist, J.A., Rapela, C.W., Baldo, E.G., Murra, J.A., Alasino, P.H., Colombo, F., 2011. Stock monzogranítico El Chorro (sierra de Ancasti, Catamarca): un ejemplo de magmatismo tipo S con granate ígneo. Revista de la Asociación Geológica Argentina 68, 195–204.

de La Roche, H. (1992). Un homologue cationique du triangle Q–A–P (quartz–feldspath alcalin–plagioclase), figure majeure de la pétrologie des roches plutoniques. Comptes Rendus de l'Academie des Sciences, Paris, 315. Serie II 1687–1693.

DePaolo, D.J., Linn, A.M., Schubert, G., 1991. The continental crustal age distribution: methods of determining mantle separation ages from Sm–Nd isotopic data and application to the southwestern United States. Journal Geophysical Research 96, 2071–2088.

Dickinson, W.R., Gehrels, G.E., 2003. U-Pb ages of detrital zircons from Permian and Jurassic eolian sandstones of the Colorado Plateau, USA: paleogeographic implications. Sedimentary Geology 163, 29–66.

Dorais, M.J., Lira, R., Chen, Y., Tingey, D., 1997. Origin of biotite–apatite-rich enclaves, Achala batholith, Argentina. Contributions to Mineralogy and Petrology 130, 31–46.

Dudas, M.J., Schmitt, R.A., Harward, M.E., 1971. Trace element partitioning between volcanic plagioclase and dacitic pyroclastic matrix. Earth and Planetary Science Letters 11, 440–446.

Fujimaki, H., 1986. Partition coefficients of Hf, Zr, and REE between zircon, apatite, and liquid. Contributions to Mineralogy and Petrology 94, 42–45.

Fujimaki, H., Tatsumoto, M., Aoki, K.-i., 1984. Partition coefficients of Hf, Zr, and REE between phenocrysts and groundmasses. Journal of Geophysical Research 89, 662–672.

Gaschnig, R.M., Vervoort, J.D., Lewis, R.S., McClelland, W.C., 2010. Migrating magmatism in the northern US Cordillera: in situ U–Pb geochronology of the Idaho batholiths. Contributions to Mineralogy and Petrology 159, 863–883.
Gomes, M.E.P., Neiva, A.M.R., 2005. Geochemistry of granitoids and their minerals from Rebordelo–Agrochao area, northern Portugal. Lithos 85, 235–254.
Grosse, P., Söllner, F., Baéz, M.A., Toselli, A.J., Rossi, J.N., de la Rosa, J.D., 2009. Lower carboniferous post-orogenic granites in central-eastern Sierra de Velasco, Sierras Pampeanas, Argentina: U–Pb monazite geochronology and Sr–Nd isotopes. International Journal of Earth Sciences 98, 1001–1025.
Hanson, G.N., 1978. The application of trace elements to the petrogenesis of igneous rocks of granite composition. Earth and Planetary Science Letters 38, 26–43.
Higuchi, H., Nagasawa, H., 1969. Partition of trace elements between rock-forming minerals and the host volcanic rocks. Earth and Planetary Science Letters 7, 281–287.
Jang, Y.D., Naslund, H.R., 2003. Major and trace element variation in ilmenite in the Skaergaard intrusion: petrologic implications. Chemical Geology 193, 109–125.
Jarosewich, E.J., Nelen, J.A., Norberg, J.A., 1980. Reference samples for electron microprobe analysis. Geostandard Newsletter 4, 43–47.
Johannes, W., Ehlers, C., Kriegsman, L.M., Mengel, K., 2003. The link between migmatites and S-type granites in the Turku area, southern Finland. Lithos 68, 69–90.
Jordan, T.E., Almendinger, R.W., 1986. The sierras Pampeanas of Argentina: a modern analogue of Rocky mountain foreland deformation. American Journal of Science 286, 737–764.
Kemp, A.I.S., Whitehouse, M.J., Hawkesworth, C.J., Alarcon, M.K., 2005. A zircon U–Pb study of metaluminous (I-type) granites of the Lachlan Fold Belt, southeastern Australia: implications for the high/low temperature classification and magma differentiation processes. Contributions to Mineralogy and Petrology 150, 230–249.
Knüver, M., 1983. Dataciones radimétricas de rocas plutónicas y metamórficas. In: Aceñolaza, F.G., Miller, H., Toselli, A. (Eds.), Geología de la Sierra de Ancasti, 59. Münstersche Forschungen zur Geologie und Paläontologie, pp. 201–218.
Kretz, R., 1983. Symbols for rock-forming minerals. American Mineralogist 68, 277–279.
Ludwig, K.R., 2003. Isoplot 3.0. A Geochronological Toolkit for Microsoft Excel. Special Publication, 4. Berkeley Geochronological Center, Berkeley, CA 94709, USA.
Luhr, J.F., Carmichael, I.S.E., 1980. The Colima volcanic complex, Mexico. I: post-caldera andesites from Volcan Colima. Contributions to Mineralogy and Petrology 71, 343–372.
Matsui, Y., Onuma, N., Nagasawa, H., Higuchi, H., Banno, S., 1977. Crystal structure control in trace element partition between crystal and magma. Tectonics 100, 315–324.
McGuire, A.V., Francis, C.A., Dyar, M.D., 1992. Mineral standards for electron microprobe analysis of oxygen. American Mineralogist 77, 1087–1091.
Middlemost, E.A.K., 1994. Naming materials in the magma/igneous rock system. Earth Science Reviews 37, 215–224.
Miller, C.F., McDowell, S.M., Mapes, R.W., 2003. Hot and cold granites? Implications of zircon saturation temperatures and preservation of inheritance. Geology 31, 529–532.
Miller, H., Söllner, F., 2005. The Famatina complex (NW-Argentina): back-docking of an island arc or terrane accretion? Early Palaeozoic geodynamics at the western Gondwana margin. In: Vaughan, A.P.M., Leat, P.T., Pankhurst, R.J. (Eds.), Terrane Processes at the Margins of Gondwana, vol. 246. Geological Society of London, Special Publication, pp. 241–256.
Miller, C.F., Stoddard, E.F., Bradfish, L.J., Dollase, W.A., 1981. Composition of plutonic muscovite: genetic implications. Canadian Mineralogist 19, 25–34.
Nagasawa, H., 1970. Rare earth concentrations in zircon and apatite and their host dacite and granites. Earth and Planetary Science Letters 9, 359–364.
Nagasawa, H., Schnetzler, C.C., 1971. Partitioning of rare earth, alkali, and alkaline earth elements between phenocrysts and acidic igneous magmas. Geochimica et Cosmochimica Acta 35, 953–968.
Nakamura, N., 1974. Determination of REE, Ba, Mg, Na and K in carbonaceous and ordinary chondrites. Geochimica et Cosmochimica Acta 38, 757–773.
Nash, W.P., Crecraft, H.R., 1985. Partition coefficients for trace elements in silicic magmas. Geochimica et Cosmochimica Acta 49, 2309–2322.
Pankhurst, R.J., Rapela, C.W., Fanning, C.M., 2000. Age and origin of coeval TTG, I- and S-type granites in the Famatinian belt of NW Argentina. Transactions of the Royal Society of Edinburgh: Earth Sciences 91, 151–168.
Paces, J.B., Miller, J.D., 1993. Precise U-Pb ages of Duluth Complex and related mafic intrusions, north- eastern Minnesota: geochronological insights to physical, petrogenetic, paleomagnetic, and tectonomagmatic processes associated with the 1.1 Ga midcontinental rift system. Journal Geophysical Research 98, 13997–14013.
Pankhurst, R.J., Rapela, C.W., Saavedra, J., Baldo, E.G., Dahlquist, J.A., Pascua, I., Fanning, C.M., 1998. The Famatinian arc in the central sierras Pampeanas: an early to mid-Ordovician continental arc on the Gondwana margin. In: Pankhurst, R.J., Rapela, C.W. (Eds.), The Proto-Andean Margin of Gondwana, vol. 142. Geological Society of London, Special Publication, pp. 343–367.
Parada, M.A., 1992. Contribución a la geoquímica del Complejo Plutónico Papudo-Quintero, Chile central: implicancias petrogenéticas. Revista Geológica de Chile 19, 199–210.
Paster, T.P., Schauwecker, D.S., Haskin, L.A., 1974. The behavior of some trace elements during solidification of the Skaergaard layered series. Geochimica et Cosmochimica Acta 38, 1549–1577.
Rapela, C.W., 2000. Accretionary history and magmas sources in the Southern Andes. 31st International Geological Congress. Río de Janeiro. Brasil. Abstract Volume (CD-ROM).
Rapela, C.W., Pankhurst, R.J., Casquet, C., Baldo, E., Galindo, C., Fanning, C.M., Dahlquist, J.A., 2010. The Western Sierras Pampeanas: protracted Grenville-age history (1330–1030 Ma) of intra-oceanic arcs, subduction–accretion at continental-edge and AMCG intraplate magmatism. Journal of South American Earth Sciences 29, 105–127.
Rapela, C.W., Baldo, E.G., Pankhurst, R.J., Fanning, C.M., 2008. The Devonian Achala batholith in the Sierras Pampeanas: F-rich aluminous A-type granites. VI South American Symposium on Isotope Geology, Proceedings in CD-ROM, Paper 53. San Carlos de Bariloche, Argentina.
Rapela, C.W., Pankhurst, R.J., Casquet, C., Fanning, C.M., Baldo, E., González-Casado, J.M., Galindo, C., Dahlquist, A., 2007. The Río de la Plata craton and the assembly of SW Gondwana. Earth-Science Reviews 83, 49–82.
Rapela, C.W., Fanning, M., Baldo, E., Dahlquist, J., Pankhurst, R.J., Murra, J., 2005. Coeval S- and I-type granites in the Sierra de Ancasti, Eastern Sierras Pampeanas, Argentina. In: Pankhurst, R.J., Veiga, G. (Eds.), Gondwana 12: Geological and Biological Heritage of Gondwana, Abstract, 307.
Rapela, C.W., Pankhurst, R.J., Casquet, C., Baldo, E., Saavedra, J., Galindo, C., 1998. Early evolution of the proto-Andean margin of South America. Geology 26, 707–710.
Reissinger, M., 1983. Evolución geoquímica de la sierra de Ancasti. In: Aceñolaza, F.G., Miller, H., Toselli, A. (Eds.), Geología de la Sierra de Ancasti, vol. 59. Münstersche Forschungen zur Geologie und Paläontologie, pp. 101–112.
Saavedra, J., Toselli, A., Rossi, J., Pellitero, E., Durand, F., 1998. The early Palaeozoic magmatic record of the Famatina system: a review. In: Pankhurst, R.J., Rapela, C.W. (Eds.), The Proto-Andean Margin of Gondwana, vol. 42. Journal of the Geological Society of London, Special Publication, pp. 283–295.
Schnetzler, C.C., Philpotts, J.A., 1970. Partition coefficients of rare-earth elements between igneous matrix material and rock-forming mineral phenocrysts; II. Geochimica et Cosmochimica Acta 34, 331–340.
Siegesmund, S., Steenken, A., López de Luchi, M.G., Wemmer, K., Hoffmann, A., Mosch, S., 2004. The Las Chacras–Potrerillos batholith (Pampean Ranges, Argentina): structural evidence, emplacement and timing of the intrusion. International Journal of Earth Sciences 93, 23–43.
Sims, J.P., Ireland, T.R., Camacho, A., Lyons, P., Pieters, P.E., Skirrow, R.G., Stuart-Smith, P.G., 1998. U–Pb, Th–Pb and Ar–Ar geochronology from the southern sierras Pampeanas, Argentina: implications for the Palaeozoic tectonic evolution of the western Gondwana margin. In: Pankhurst, R.J., Rapela, C.W. (Eds.), The Proto-Andean Margin of Gondwana, vol. 142. Geological Society of London, Special Publication, pp. 259–281.
Sisson, T.W., 1991. Pyroxene-high silica rhyolite trace-element partition-coefficients measured by ion microprobe. Geochimica et Cosmochimica Acta 55, 1575–1585.
Speer, J.A., 1984. Micas in igneous rocks. Reviews in Mineralogy 13, 357–368.
Steiger, R.H., Jäger, E., 1977. Subcommission of geochronology: convention on the use of decay constants in geo- and chosmochronology. Earth and Planetary of Science Letters 1, 369–371.
Stuart-Smith, P.G., Miró, R., Sims, J.P., Pieters, P.E., Lyons, P., Camacho, A., Skirrow, R.G., Black, L.P., 1999. Uranium-lead dating of felsic magmatic cycles in the southern Sierras Pampeanas, Argentina: implications for the tectonic development of the proto-Andean Gondwana margin. In: Ramos, V.A., Keppie, J.D. (Eds.), Laurentia-Gondwana Connections before Pangea, 336. Geological Society of America Special Publication, pp. 87–114.
Vance, J.A., 1962. Zoning in igneous plagioclase: normal and oscillatory zoning. American Journal of Science 260, 746–760.
Vervoort, J.D., Blichert-Toft, J., 1999. Evolution of the depleted mantle: Hf isotope evidence from juvenile rocks through time. Geochimica et Cosmochimica Acta 63, 533–556.
Villemant, B., Jaffrezic, H., Joron, J.L., Treuil, M., 1981. Distribution coefficients of major and trace-Elements - Fractional crystallization in the alkali Basalt series of Chaine-Des-Puys (Massif central, France). Geochimica et Cosmochimica Acta 45, 1997–2016.
Walker, J.A., Carr, M.J., 1986. Compositional variations caused by phenocryst sorting at Cerro Negro volcano, Nicaragua. Geological Society of American Bulletin 97, 1156–1162.
White, A.J.R., Chappell, B.W., 1977. Ultrametamorphism and granitoids genesis. Tectonophysics 43, 7–22.
Williams, I.S., 1998. U–Th–Pb geochronology by ion microprobe. In: McKibben, M.A., Shanks, W.C. (Eds.), Applications of Microanalytical Techniques to Understanding Mineralising Processes, vol. 7. Reviews in Economic Geology, pp. 1–35.
Willner, A., 1983a. Evolución metamórfica. In: Aceñolaza, F.G., Miller, H., Toselli, A. (Eds.), Geología de la Sierra de Ancasti, vol. 59. Münstersche Forschungen zur Geologie und Paläontologie, pp. 189–200.
Willner, A., 1983b. Evolución tectónica. In: Aceñolaza, F.G., Miller, H., Toselli, A. (Eds.), Geología de la Sierra de Ancasti, vol. 59. Münstersche Forschungen zur Geologie und Paläontologie, pp. 157–187.